10 September 1965, Volume 149, Number 3689 SCIENCE

EDITORIAL CORRESPONDENCE: 1515 Massachusetts Ave., NW. Washington. D.C. 20005. Phone: 202-387-7171. Cable: Advancesci. Washington. Copies of "Instructions for Contributors" can be obtained from the editorial office. ADVERTISING CORRESPONDENCE: Rm. 1740. 11 W. 42 St., New York, N.Y. 10036. Phone: 212-PE 6-1858.

Mariner IV Mission

Scientifically, the results of the Mariner IV mission constitute the most important advance in space research since the discovery of the Van Allen radiation belts. Contributing to the value of the mission is the fact that the results of the various experiments are complementary; they also build on and extend previous findings of ground-based astronomy.

Useful data on particles, fields, and micrometeorites were collected during the voyage to Mars. Additional information was gathered after the fly-by, and more may be forthcoming when the spacecraft is once again fairly close to Earth. The major contributions, however, are the observations in the vicinity of Mars. Among the most important are the photographs (*Science*, 6 August). These show that, unlike Earth, Mars resembles the moon in topography. There are many craters, but there is no evidence of mountain chains.

Experiments on particles and fields reported in this issue show other major differences between the two planets. The magnetic field of Mars is not more than 1/1000 that of Earth, and the Red Planet has no radiation belt. An occultation experiment gives independent evidence that the atmosphere of Mars is tenuous and unlike that of Earth. A micrometeorite study shows that interplanetary dust is more abundant in the vicinity of Mars than near Earth.

The evidence from the photographs, the absence of a sizable magnetic field, and the character of the atmosphere all support the view that the history of Mars has been unlike that of Earth.

An example of a close relation between Earth-based findings and findings from Mariner is the estimate of the composition and density of the Martian atmosphere. Astronomers have known for some time that the atmosphere of Mars is thin and that it contains CO_2. Recently the estimates have been sharpened. Measures of infrared radiation indicate that the total pressure at the Martian surface is 11 millibars, of which about half is CO_2 (0.28 mole per square centimeter). The Mariner IV occultation experiment determined changes in radio signals from the spacecraft caused by passage through the atmosphere and the ionosphere of Mars. Preliminary interpretation of the data provides an estimate of the scale height of the atmosphere (~9 km) and its density. The pressure at the surface of Mars as estimated from the data (about 5 or 6 mb) is lower than estimates obtained in ground-based studies. This disagreement is not serious, and the discrepancy will probably diminish on further analysis. The important fact is that two very different kinds of measurements give essentially the same result. Half or more of the atmosphere of Mars is CO_2, and the total number of molecules per unit area is about 1/100 the number in the Earth's atmosphere.

The contrast between Earth and Mars can be stated in another way by listing the amounts per unit area of three volatile substances that have appeared at the surface of the planets in the past or are now present. For Earth the values are: H_2O, 3.2×10^5 g; CO_2, 1.8×10^4 g; N_2, 8×10^2 g. The corresponding values for Mars are: H_2O, ~0.01 g; CO_2, ~12 g; N_2, <10 g. The numbers are not strictly comparable, for most of the CO_2 that has reached the surface of the Earth is now incorporated in sedimentary rocks. Probably most of the H_2O that has appeared on Mars has been lost, the hydrogen having escaped and the oxygen having been consumed or lost. Nitrogen has not been detected on the planet, and the value given is probably an upper limit, derived from the pressure effect it exerts on CO_2.

The success of Mariner IV represents a superb engineering achievement by the Jet Propulsion Laboratory. The accomplishment required the proper functioning of 134,000 parts after 7 months in space. The magnitude of the success is highlighted by the failure of others to attain the goal. The Russians, who have some first-class engineering talent, have not succeeded in their dozen or so attempts at attaining close-in data from Mars or Venus.—PHILIP H. ABELSON

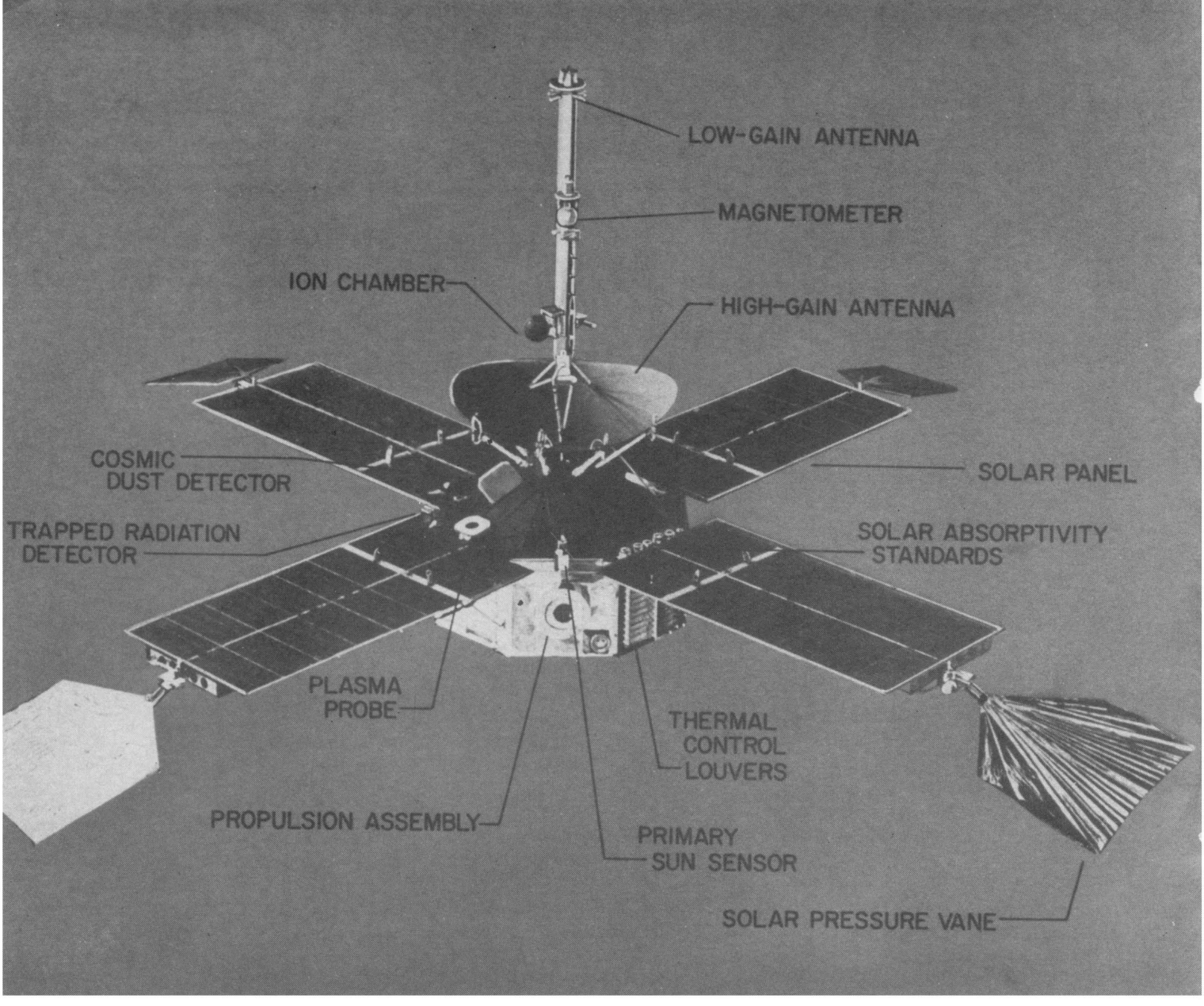

Mariner Mars spacecraft looking counter to its direction of motion around the sun. The rod-like omnidirectional antenna waveguide points toward the sun. The greatest dimension, between ends of the "Solar vanes," is 6.9 m. [Jet Propulsion Laboratory–National Aeronautics and Space Administration]

Mariner IV Measurements near Mars: Initial Results

Spacecraft Description and Encounter Sequence

The Mariner IV spacecraft was launched from Cape Kennedy at 1422 Universal Time, 28 November 1964, and power was applied to the "fields-and-particles" experiments at 1507. Data from these experiments have returned to Earth continuously since that time, except during commanded operations such as the midcourse correction, until 1154 U.T., 15 July 1965, when transmission of the tape-recorded pictures of Mars began. Initial results of the television experiment are described by Leighton *et al.* (*1*). In the following reports measurements made of the magnetic field and the various particle fluxes near Mars during the approximately 24 hours preceding picture transmission are described. The final report describes the occultation experiment, in which the behavior of the radio signal transmitted by the spacecraft as it passed behind Mars is used to infer properties of the planet's atmosphere.

With the exceptions of the TV system and portions of the data automa-

tion system (DAS), the spacecraft and the experiments operated in the same way during encounter as during the cruise phase of the mission. The attitude of the spacecraft has been controlled throughout the flight since roll stabilization at 0710, 29 November 1964, by optical sensors and cold gas jets.

The roll axis of the spacecraft is aligned with the radial vector from the sun so that the solar panels remain normal to this vector. Orientation about the roll axis is maintained by keeping the spacecraft aligned so that an optical sensor, whose axis is approximately perpendicular to the roll axis, points at the bright star Canopus, near the south ecliptic pole. In this attitude the beam of the fixed, directional antenna lies approximately in the plane of the ecliptic and was pointed continuously at Earth from 5 March through encounter. The attitude-control gyros were used only during certain operations early in the mission; the optical sensors kept the spacecraft stabilized within 0.5° at all other times.

The spacecraft transmits 10 watts at a frequency of 2300 Mcy/sec; it employed an information rate of 33⅓ bit/sec from launch to 1700 U.T., 3 January 1965, and 8⅓ bit/sec thereafter. At the latter rate, the basic data cycle, consisting of 280 bits of science data and 140 bits of engineering data, occupies 50.4 sec. The DAS conditions and commutates data from the six experiments into these "data frames." Four three-axis magnetic measurements are telemetered in each such frame; the cosmic-dust detector and cosmic-ray telescope require two frames for each complete measurement, the ion chamber requires four, the trapped-radiation detector eight, and the solar-plasma detector 36. Only the TV camera data are stored on board.

The entire spacecraft weighs 261 kg and consumes about 170 watts in the cruise mode of operation. About 340 watts are generated by the solar cells at Earth's orbit. The six fields-and-particles experiments and the DAS weigh 21.3 kg and use 15.4 watts. The instruments are located as follows:

Magnetometer: on the waveguide leading to the omnidirectional antenna.

Ion chamber: on the waveguide leading to the omnidirectional antenna, nearer the body of the spacecraft.

Table 1. Areocentric equatorial coordinates of Mariner IV. The coordinates are centered on Mars, and the principal plane is Mars's equator. Local time is computed by use of 15° longitude per hour.

Position of observation	U.T. at Earth	Radial distance (km)	Latitude (deg)	Local time (hr)	Sun-Mars-probe angle (deg)
		14 July			
Incoming asymptote	<1812	>116,000	+8	0946	34
Cross equatorial plane	2207	53,400	0	1000	33
		15 July			
Cross noon meridian	0052	14,500	−49	1200	65
Closest approach	0113	13,200	−65	1442	86
Enter occultation	0231	25,800	−31	2058	136
Exit occultation	0325	39,300	−20	2122	142
Outgoing asymptote	>1012	>147,500	− 5	2150	146

Trapped-radiation detector: on body, with counter-axes pointing 70° and 135° from the solar direction.

Comic-ray telescope: inside body, pointing in antisolar direction.

Solar plasma detector: on body, pointing 10° from the solar direction.

Cosmic-dust detector: on body, with microphone plate approximately perpendicular to plane of orbit. The spacecraft has been fully described (*2*).

The ion chamber ceased functioning on 17 March. The other five experiments operated through encounter as they did in the cruise mode. The special events in the encounter sequence (U.T.) are as follows: 14 July, 1453, turn on TV camera; 2235, switch to encounter-data mode, which commits entire 420-bit frame to scientific instruments, adding additional cosmic-ray telescope, magnetometer, and plasma samples to each frame; 15 July, 0030, start taking TV pictures; 0055, stop taking TV pictures; 0055, return to cruise-data mode; 0113, closest approach to Mars; 0231, enter occultation; 0325, exit occultation; 1154, start picture transmission (cruise experiments off). The signals from the spacecraft propagated from Mars to Earth in 12 minutes.

Mariner IV's elliptical interplanetary orbit was inclined 0.12° to the ecliptic, with perihelion near Earth at launch and aphelion near Mars at encounter. Mars overtook the spacecraft (in ecliptic longitude) in such a way that in an areocentric system the spacecraft

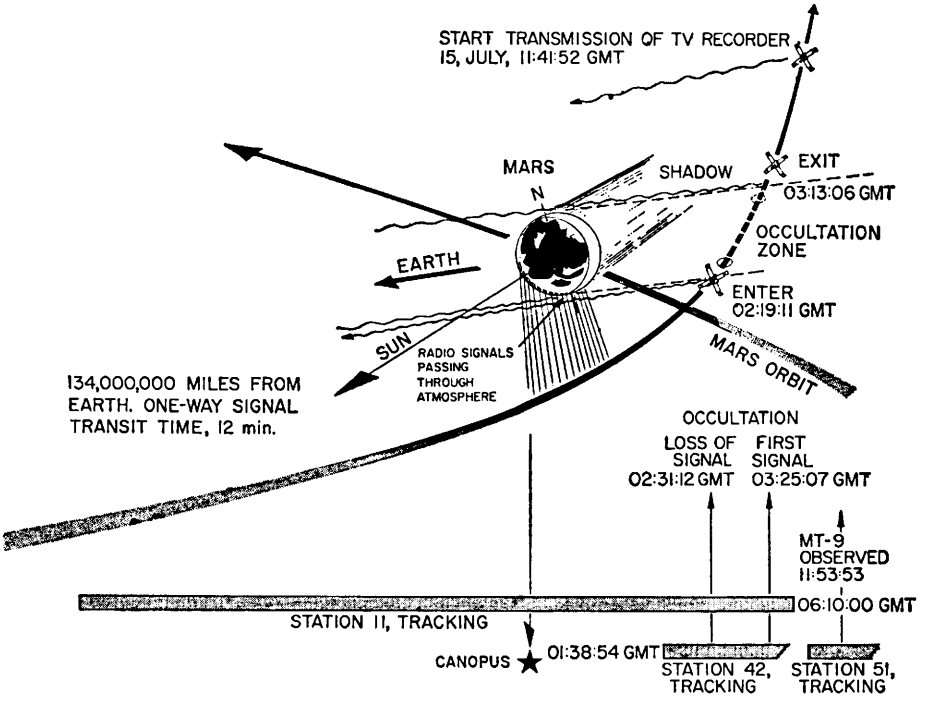

Fig. 1. Mariner IV encounter sequence and trajectory.

approached the planet at 4.5 km/sec from a local time of 0946 and nearly in the plane of Mars's orbit (Fig. 1). Mars's orbit is inclined 1°51′ to the ecliptic, and its equatorial plane makes an angle of 25°12′ with its orbital plane. On 14 July, Mars's north pole was tipped in the direction of orbital motion and toward the sun so that the subsolar point lay at 15.3°N latitude. Mars was 216 × 10^6 km from Earth, 232 × 10^6 km from the Sun (1.55 AU), and the Earth-Sun-Mars angle was 64°. The spacecraft passed over Mars's southern hemisphere. Shortly after the time of closet approach, it passed behind the planet as seen from Earth ("occultation"), but without entering the shadow of the planet. Some useful trajectory parameters appear in Table 1.

The fields-and-particles experiments were turned off during picture transmission from 1154, 15 July, to 2 August. Interplanetary results obtained before encounter and after 2 August will not be reported now.

HUGH R. ANDERSON
Jet Propulsion Laboratory,
Pasadena, California

References and Notes

1. R. B. Leighton, B. C. Murray, R. P. Sharp, J. D. Allen, R. K. Sloan, *Science* **149**, 627 (1965).
2. J. R. Casani, A. G. Conrad, R. A. Neilson, *Astronaut. Aeronaut.* 3, 16 (1965); J. D. Schmuecker and J. N. Wilson, *ibid.*, p. 26; J. N. James, *ibid.*, p. 34; W. S. Shipley and J. E. Maclay, *ibid.*, p. 42; R. A. Welnick and F. H. Wright, *ibid.*, p. 50.
3. The Mariner IV project was managed by JPL/CIT for NASA under contract NAS7-100.

16 August 1965

Absence of Martian Radiation Belts and Implications Thereof

Abstract. *A system of sensitive particle detectors on Mariner IV showed the presence of electrons of energy (E_e) less than 40 kiloelectron volts out to a radial distance of 165,000 kilometers in the morning fringe of the earth's magnetosphere but failed to detect any such electrons during the close encounter with Mars on 14–15 July 1965, at the time when the minimum areocentric radial distance was 13,200 kilometers. This result can mean that the ratio of the magnetic dipole moment of Mars to that of the earth (M_M/M_E) is surely less than 0.001 and probably is less than 0.0005. The corresponding upper limits on the equatorial magnetic field at the surface of Mars are 200 and 100 gammas, respectively. It appears possible that the solar wind interacts directly with the Martian atmosphere.*

There is not yet a quantitative theory of the origin of the earth's radiation belts despite a large body of observational knowledge on (i) the distributions and energy spectra of the constituent particles and the time variations thereof; (ii) the geomagnetic field and its variations; (iii) natural radio waves in the ionosphere; (iv) the atmosphere of the earth; and (v) the solar wind in its vicinity. Thus it is clearly impossible to predict the detailed nature of the radiation belts of a planet of arbitrary magnetic moment at an arbitrary distance from the sun. Nonetheless it is apparent that the planet must be magnetized sufficiently strongly and it must be exposed to the flow of hot, ionized gas from the sun (the solar wind) in order that it have radiation belts resembling those of the earth. Under the latter requirement we are neglecting the minor component of the earth's radiation belts due to the radioactive-decay products of cosmic-ray-produced neutron albedo. Since the earth at 1.0 AU (astronomical unit, or 1.495985 × 10^8 km) and Jupiter at 5.2 AU from the sun both have intense radiation belts it is reasonable to expect that Mars at the intermediate distance of 1.52 AU has radiation belts also, *if it is a sufficiently magnetized body*. The criterion for sufficiency, in approximate terms, is that the outward pressure of the planet's magnetic field ($B^2/8\pi$) equals the inward dynamic pressure of the solar wind (nmv^2) at a radial distance R exceeding that to the top of its appreciable atmosphere. In the foregoing, B denotes the magnetic field strength ($B \sim M/R^3$); and n is the number density of charged particles of mass m and directed velocity v in the solar wind. In the case of the earth (magnetic dipole moment $M_E = 8.06 \times 10^{25}$ gauss cm^3), the stagnation point occurs at a radial distance of some 65,000 km on its sunward side.

Understanding of the configuration of the external magnetic field of a planet subjected to the flow of the solar wind dates from the classical theoretical work of Chapman and Ferraro in the 1930's. In recent years, this understanding has been improved by advances in the theory and endowed with detailed physical validity by a large variety of satellite and space-probe observations.

Not so clearly anticipated by the theory have been the observational findings (*1–3*) of the presence of electrons having energies of the order of tens of kev in the transition region between the (hypersonic) shock front and the magnetopause, and in the magnetospheric tail (in addition to the now well-known distribution of durably trapped electrons and protons interior to the magnetopause).

Outside of the shock front, the presence of the earth is undetectable by either magnetic measurements (*4*) or particle measurements (*2*). Within the transition region, there are turbulent magnetic fields of the order of 30 gammas (1 gamma = 10^{-5} gauss) (*5*) and an irregular distribution of electrons having energies from ~1 kev to some tens of kev. Interior to the magnetopause, there are regular magnetic fields and large intensities of durably trapped electrons and protons of energies up to several Mev.

On the strength of this massive observational knowledge of the earth's environment and of supporting theoretical considerations (*6*), it is assumed here that the appearance of detectable intensities of electrons having energies of some tens of kev is an inevitable and universal consequence of the quasi-thermalization of the solar wind (collisionless conversion of directed kinetic energy into random kinetic energy) as its forward motion is arrested by impact against a planetary magnetic field.

To the extent that this assumption is valid, a sensitive magnetometer and a sensitive detector of low-energy electrons are equivalent devices for the detection of a planetary magnetic field.

The search for radiation belts of Venus and of Mars was proposed in detail by us in 1959. Our simple low-energy-electron detector was carried on Mariner II which flew past Venus on 14 December 1962 at a minimum radial distance of approach of 41,000 km on the sunward side of the planet. No planetary effect was detected. This negative result was originally inter-

preted (*7*) to mean that the ratio of the magnetic dipole moment of Venus to that of the earth $M_V/M_E \leq 0.18$. A recent reinterpretation based on subsequently increased knowledge of particle distributions in the earth's transition region, suggests $M_V/M_E \leq 0.1$ (*8*).

The University of Iowa "package" of low-energy-particle detectors on Mariner IV comprises three end-window Geiger-Mueller tubes (EON type 6213), designated A, B, and C, and one thin (35-micron) surface-barrier solid-state detector (Nuclear Diodes, Inc.) having two discrimination levels, designated D_1 and D_2. Each of the four detectors has a conical collimator with a full vertex angle of 60° (nominal). The axes of the collimators of B, C, and D are parallel to each other and at an angle of 70° to the roll axis of the spacecraft, and the axis of the collimator of A is at an angle of 135°. The roll axis of the spacecraft is directed continuously at the sun with an error of less than 1°; rotation of the spacecraft about this axis is controlled so that the axis of a spacecraft-fixed, directional antenna is pointed approximately toward the earth. Thus, detectors B, C, and D receive particles moving generally outward from the sun and at angles to the sun-to-probe vector of 70° ± 30°. The detectors themselves and the complete inner walls of their collimators are shielded from direct light and x-rays from the sun. Detector A receives particles moving generally inward toward the sun at angles to the sun-to-probe vector of 135° ± 30°. The sidewall shielding of all detectors has a minimum thickness corresponding to the range of ~50-Mev protons. Both discrimination levels of the solid-state detector, D_1 and D_2, are insensitive to electrons of any energy in the intensities found in the present series of experiments. This insensitivity is designed into the system (thin detector, high bias level, and 200-nsec delay-line pulse-clipping) and was demonstrated in thorough testing prior to flight. It was further confirmed during traversal of the magnetosphere in the early phase of the flight of Mariner IV (*9*). Detector channels D_1 and D_2 are also insensitive to galactic cosmic rays. In order to have direct observational knowledge of the proper operation of these channels during interplanetary flight, the solid-state detector is equipped with an $_{95}AM^{241}$ source of ~5.5-Mev alpha particles

Table 1. Characteristics of detectors.

Detector	Geometric factor: Unidirectional (cm² sterad)	Geometric factor: Omnidirectional (cm²)	Particles to which sensitive: Electrons (E_e)	Particles to which sensitive: Protons (E_p)	Dynamic range
A	0.044 ± .005	~ 0.15	≳ 45 kev	>670 ± 30 kev	From galactic cosmic ray rate of 0.6 to 10^7 count/sec
B	.055 ± .005	~ .15	≳ 40 kev	>550 ± 20 kev	As for A
C	.050 ± .005	~ .15	≳ 150 kev	>3.1 Mev	As for A
D_1	.065 ± .003		None	$0.50 \leq E_p \leq 11$ Mev	From inflight source rate to 10^6 count/sec
D_2	.065 ± .003		None	$0.88 \leq E_p \leq 4.0$ Mev	As for D_1

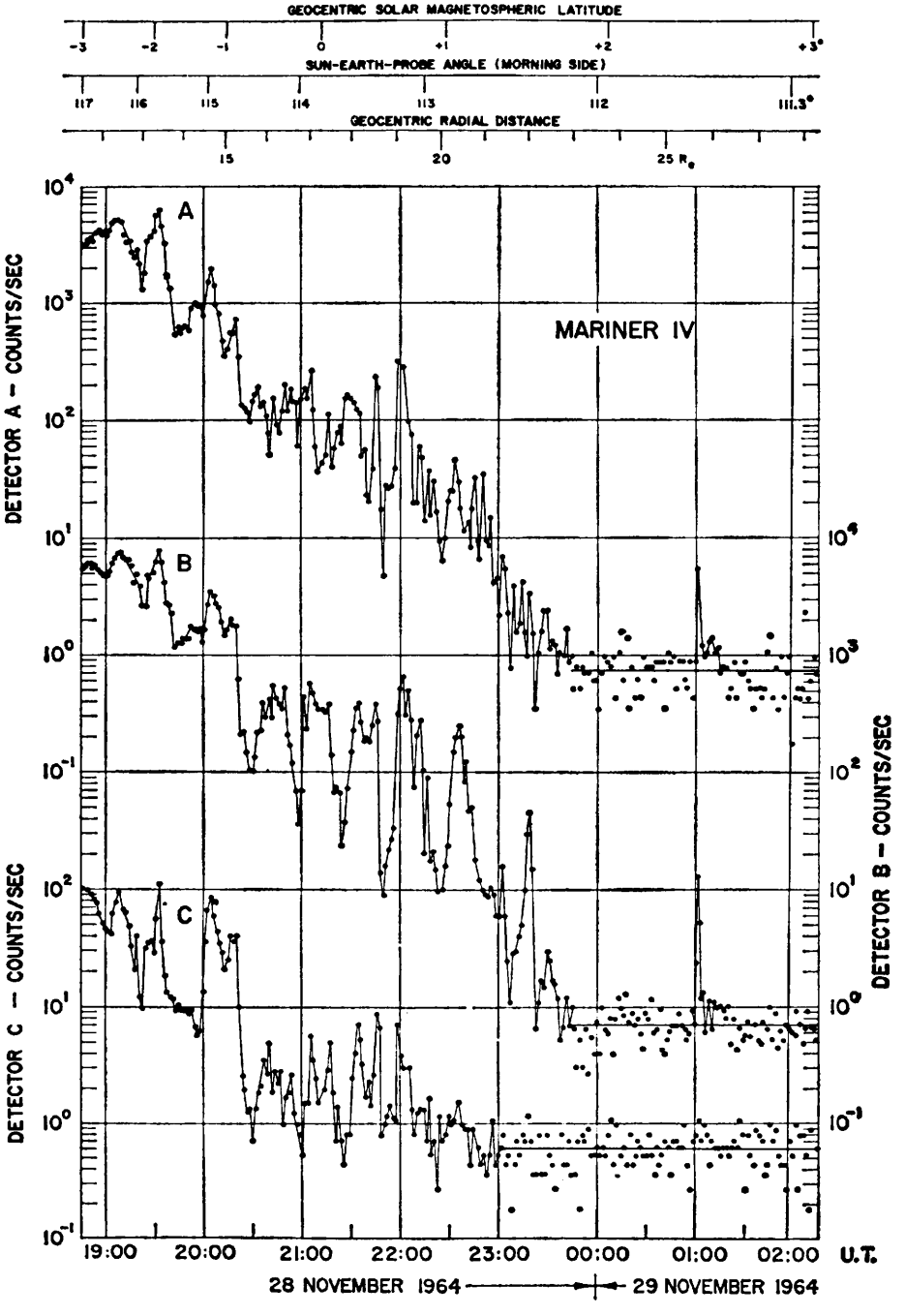

Fig. 1. Counting rates of detectors A, B, and C on Mariner IV during outward traversal of earth's magnetosphere.

which provides in-flight counting rates of 0.071 and 0.059 sec^{-1} on D_1 and D_2, respectively—rates which are accurately identical to their values before launch.

The counting rate of each of the three Geiger tubes is the sum of the rates due to galactic cosmic rays (about 0.6 count/sec); to electrons, x-rays, protons, alpha particles, and other particles, which pass through their collimators; and, in some cases, to sidewall penetrations.

Further details concerning the detectors are given in Table 1. Combinations of the data from this simple system of detectors provide information on absolute intensities, particle identification, energy spectra, and angular distributions. In favorable cases particle identification is conclusive.

The five University of Iowa data channels are part of a commutated sequence of eight as follows: E, B, D_1, D_2, E, B, A, C (where E represents the data channel from another experiment). The basic frame of telemetry during the "cruise mode" (8.33 bit/sec for entire spacecraft), which was employed throughout the period of the present study, is of 50.4-second duration. Unscaled counts from each of the detectors corresponding to the above eight channels are gated in turn into a shift register of 19 bits plus 2 overflow bits for a 45.0-second period and are read out through the spacecraft telemetry system during the subsequent 5.4 seconds. A complete cycle of eight detectors is completed each 8 × 50.4, or 403.2 seconds. Thus the "duty cycle" of each of the four channels A, C, D_1, and D_2 is 11.2 percent and that of channel B is 22.3 percent.

Outward Passage through the Earth's Magnetosphere. Of the four detectors in our (University of Iowa) equipment, the low-energy-electron detectors, A and B, are the most sensitive for the detection of the outer fringes of a magnetosphere.

The outward traversal of the earth's magnetosphere by Mariner IV on 28–29 November 1964 provides a basic calibration of the capabilities of the system and the direct foundation for the interpretation of the observations during the Martian encounter. The responses of detectors A, B, and C during the traversal of the morning fringe of the earth's magnetosphere are shown in Fig. 1. The intensity of protons $0.5 \leqq E_p \leqq 11$ Mev (D_1) drops to an undetectable level at a radial distance of 10.5 R_E (earth radii) (*9*)—not shown in Fig. 1—but electrons of energy $E_e > 40$ kev are detected continuously out to 23 R_E and there is an outlying intensity spike at 25.7 R_E. The unidirectional geometric factors of detectors A and B on Mariner IV (Table 1) are over 20 times as great as those of similar low-energy-electron detectors used by this laboratory in Explorer XIV (*10*) and OGO-I and by Anderson *et al.* (*3*) in IMP's I, II, and III (interplanetary monitoring plat-

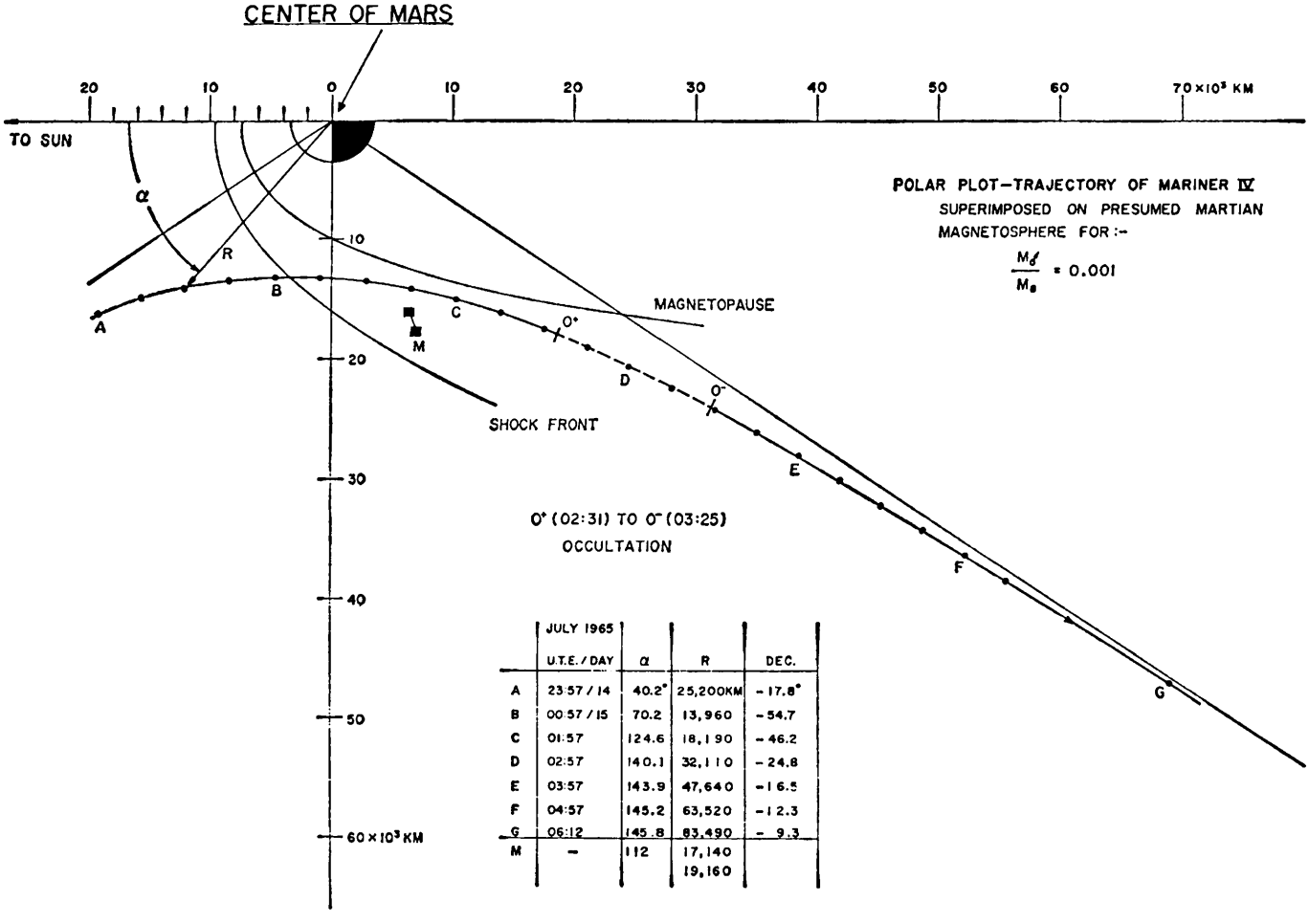

	JULY 1965 U.T.E. / DAY	α	R	DEC.
A	23:57 / 14	40.2°	25,200KM	-17.8°
B	00:57 / 15	70.2	13,960	-54.7
C	01:57	124.6	18,190	-46.2
D	02:57	140.1	32,110	-24.8
E	03:57	143.9	47,640	-16.5
F	04:57	145.2	63,520	-12.3
G	06:12	145.8	83,490	-9.3
M	-	112	17,140 19,160	

Fig. 3. An analytical diagram used for inferring an upper limit to the ratio of the magnetic dipole moment of Mars to that of the earth. Successive black dots on the trajectory are at 15-minute intervals.

forms). Their omnidirectional geometric factors are, however, about the same. Hence the detectors on Mariner IV have a 20-fold increase in "signal-to-noise ratio" for the detection of electrons having energies of the order of some tens of kev.

We noted that the outermost detectable limit of the earth's magnetosphere (25.7 R_E at a Sun-Earth-probe angle of 112°) as shown by our detectors A and B is nearly the same as that reported by Ness *et al.* (*4*) with the IMP-I magnetometer.

Encounter with Mars. The Martian encounter occurred on 14–15 July 1965, after 228 days of interplanetary flight during which our apparatus operated properly and provided a large volume of data on solar proton and electron events (*11*).

Every data point from each of the detectors A, B, C, D_1, and D_2 is shown in Fig. 2 for the time period 1000 U.T.E. of 14 July 1965 to 1154 U.T.E. of 15 July 1965, together with scales of areocentric latitude and areocentric radial distance R. The abbreviation U.T.E. means Universal Time Earth, that is, the Greenwich Mean Time of reception of the data at the earth; the data were recorded at the spacecraft 12.0 minutes earlier. Areocentric latitude is measured positive north and negative south from the equatorial plane of the planet (the plane through its center perpendicular to its axis of rotation). Closest approach of Mariner IV to the center of Mars, areocentric radial distance 13,200 km, occurred at 0113 U.T.E. of 15 July. During the period 0231 to 0325 U.T.E. of 15 July the spacecraft, as viewed from the earth, was occulted by Mars and no signals were received.

Prior to 1520 U.T.E. of 14 July the counting rates of all detectors were indistinguishable from their long-term interplanetary background values. At 1520 (±10) U.T.E. the rates of D_1, D_2, and B began to depart from their background values and continued clearly above background until spacecraft "science" was turned off at 1154 U.T.E. of 15 July. The effect was weak or absent on detectors A and C. The particles responsible for the effect are identified conclusively as protons (or other heavy particles) with an energy spectrum which falls steeply between 0.5 and 0.9 Mev. At the time of onset of the effect, the spacecraft was 162,000 km from the center of the planet at a Sun-Mars-probe angle of 34°. It is concluded that the observed protons are not associated with Mars on the following grounds:

1) The time (and spatial) dependence of the intensity as measured along the trajectory of the spacecraft is quite different from that expected in a planetary radiation belt.

2) No such intensities of protons are found beyond about 65,000 km from the earth in any direction; and, as will be shown below, the particle populations much nearer to Mars are vastly less than those at similar distances from the earth.

3) Both observationally and theoretically the outer fringe of a planetary magnetosphere is characterized by energetic electrons, not by protons.

4) The time history, proton intensity, and proton spectrum observed on 14–15 July are all similar to those commonly observed in interplanetary space remote from any celestial body. Five events of this nature were observed during the 2 weeks before the Martian encounter period.

For the above reasons, the observed protons on 14–15 July are identified as a "solar proton event" whose appearance during this period was coincidental with the Martian encounter.

Throughout the remainder of the encounter period, there was no further significant departure from background rates by any one of the five detector channels, A and B being presumably the most sensitive to the fringe of a magnetosphere.

Thus, no particle effects whatever, attributable to Mars, were detected despite the close approach of the spacecraft.

More precisely, the unidirectional intensity of electrons $E_e > 40$ kev did not exceed 6 (cm² sec sterad)$^{-1}$ over any 45-second sampling period. A similar trajectory past the earth would have encountered unidirectional intensities as high as 10^7 (cm² sec sterad)$^{-1}$ (*12*). Hence, as a purely observational matter it is clear that the radiation environment of Mars is vastly different from that of the earth.

Implications of the Absence of Radiation Belts. Assuming the applicability of the composite theoretical-observational knowledge of the magnetospheric transition region around the earth (described above) to that of a planet of much smaller magnetic moment, we can use our negative results to place an upper limit on the magnetic moment of Mars.

The basic scaling law (*13*) is given by

$$nmv^2 \approx B^2/8\pi \approx M^2/R^6. \quad (1)$$

It is further supposed that v at Mars is the same as at the earth and that n is an inverse square function of heliocentric radial distance. Thus, it is supposed that the shock front and the magnetopause have the same geometric shapes as for the earth with the linear scale factor

$$R_M/R_E = 1.1\ (M_M/M_E)^{\frac{1}{3}}. \quad (2)$$

It is known that the shock front and the magnetopause have approximately cylindrical symmetry about the Sun-planet line, more or less independent of the orientation of the magnetic moment of the planet.

The application of these ideas to the present situation is described by Fig. 3. The curved line ABCDEFG represents the encounter trajectory of Mariner IV in areocentric polar coordinates R (radial distance from center of Mars) and α (Sun-Mars-probe angle). The cross section of the body of the planet is shown to the same scale. Data for the trajectory plot are from Jet Propulsion Laboratory's "IBSYS-JPTRAJ-SFPRO 062965 Mariner IV Mission Encounter Fine Print 0310 GMT 15 July 61 Special," which is the first-order-corrected, post-encounter ephemeris, believed to be in error by less than 100 km. Adopting a blended best fit to present knowledge of the geometric forms of the earth's shock front and magnetopause (*2, 4, 14*), we have drawn in Fig. 3 geometrically similar curves scaled according to Eq. 2 for the case $M_M/M_E = 0.001$. The two connected squares labeled M are similarly transformed points from Fig. 1 which represent the positions of easily detectable intensities of electrons $E_e >$ 40 kev at 23.0 and 25.7 R_E, respectively, in the fringe of the earth's magnetosphere on 28–29 November 1964.

We conclude from Fig. 3 that M_M/M_E is surely less than 0.001. In fact, a literal interpretation of Fig. 3 gives $M_M/M_E < 0.0005$. In view of the wide ranges of areocentric latitude

and of α while the spacecraft was flying more or less parallel to the scaled magnetopause, these conclusions are probably valid for any orientation of the Martian magnetic moment.

The foregoing results mean that the equatorial surface magnetic field of Mars is less than 200 (and perhaps 100) gammas (radius = 3417 km), and hence they suggest that the solar wind will, on occasion and perhaps usually, have a direct interaction with the Martian atmosphere. This interaction may be of essential importance in determining the physical state of the atmosphere.

Also, it is evident that the Martian atmosphere and surface are exposed to the full effects of solar and galactic cosmic radiation irrespective of latitude.

The observed weakness of the Martian magnetic field will presumably contribute to the understanding of the internal structure of the planet, though we do not pretend competence in this field and make only a few general remarks. It is noted that the origin of the earth's general magnetic field is not understood on the basis of a priori theory and that no significant prediction of the magnetic moment of any other celestial body exists. On the basis of the most widely accepted conjecture on the physical origin of the geomagnetic field, primarily due to Bullard and to Elsasser [the subject is reviewed by Elsasser (*15*) and by Cowling (*16*)], it is believed necessary that a planetary body be endowed with both rotation and a liquid, electrically conducting core in order that its externally apparent magnetization exceed the mean of

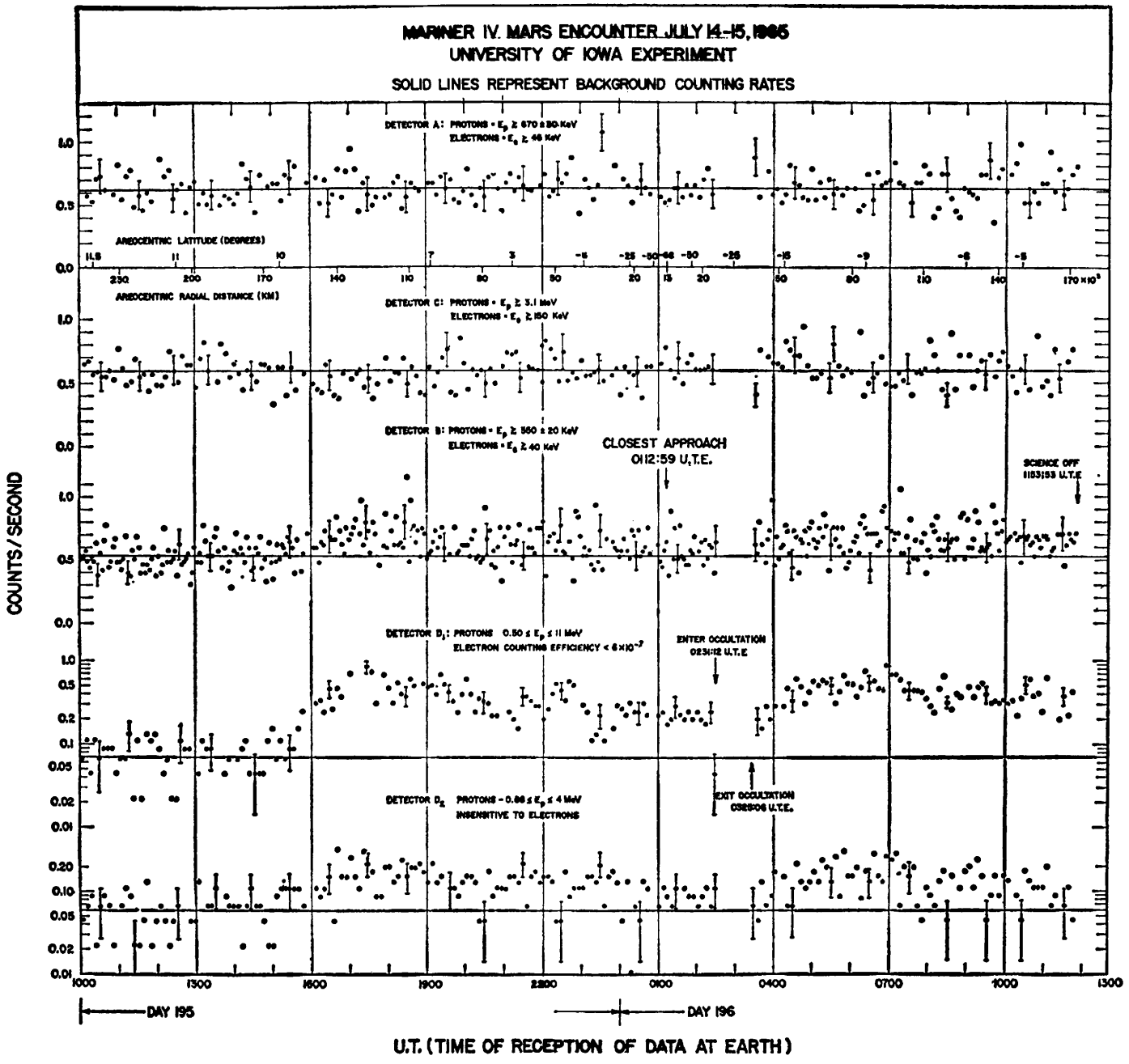

Fig. 2. A comprehensive plot of the counting rates of detectors A, C, B, D_1, and D_2 before, during, and after the encounter with Mars on 14–15 July 1965. Note scale of positional coordinates of the spacecraft in upper part of the figure.

the remanent values of its constituents. The mass of Mars is 0.107 that of the earth, its mean density is 3.95 g cm^{-3} (0.71 that of the earth and 1.18 that of the moon), and its radius is 0.536 that of the earth and 1.97 that of the moon (*17*). But since the period of rotation of Mars, 24.62 hours, is nearly the same as that of the earth, it appears that its vastly weaker magnetic moment must be attributed to such a markedly different internal structure or composition, or both, that it does not possess a liquid, electrically conducting core.

Some years ago Blackett (*18*) wrote as follows: "It has been known for a long time, particularly from the work of Schuster, Sutherland and H. A. Wilson, though lately little regarded, that the magnetic moment P and the angular momentum U of the earth and sun are nearly proportional, and that the constant of proportionality is nearly the square root of the gravitational constant G divided by the velocity of light c. We can write, in fact,

$$P = \beta \frac{G^{\frac{1}{2}}}{c} U, \qquad (4)$$

where β is a constant of the order of unity."

He (*18, 19*) considered available evidence on the angular momenta and magnetic moments of the earth, of the sun, and of five stars and was led to the following: ". . . It is suggested tentatively that the balance of evidence is that the above equation represents some new and fundamental property of rotating matter. Perhaps this relation will provide the long-sought connexion between electromagnetic and gravitational phenomena."

Blackett's hypothesis has continued to be of interest, despite the fact that it has not gained general acceptance. The present experiment on the magnetic moment of Mars provides, perhaps, the first conclusive test of the hypothesis:

The ratio of the angular momentum of Mars to that of the earth is ~0.03 and by Blackett's Eq. 4 (*18*) this is also the predicted ratio of M_M/M_E, a value which is some 30 times larger than the upper limit which we have inferred from the observational evidence.

J. A. Van Allen
L. A. Frank
S. M. Krimigis
H. K. Hills

Department of Physics and Astronomy, University of Iowa, Iowa City

References and Notes

1. J. W. Freeman, J. A. Van Allen, L. J. Cahill, *J. Geophys. Res.* **68**, 2121 (1963); C. Y. Fan, G. Gloeckler, J. A. Simpson, *Phys. Rev. Letters* **13**, 149 (1964); L. A. Frank, *J. Geophys. Res.* **70**, 1593 (1965).
2. L. A. Frank and J. A. Van Allen, *J. Geophys. Res.* **69**, 4923 (1964).
3. K. A. Anderson and H. K. Harris, *Trans. Amer. Geophys. Union* **46**, 119 (1965); ———, R. J. Paoli, *J. Geophys. Res.* **70**, 1039 (1965).
4. N. F. Ness, C. S. Scearce, J. B. Seek, *J. Geophys. Res.* **69**, 3531 (1964).
5. L. J. Cahill and P. G. Amazeen, *ibid.* **68**, 1835 (1963).
6. F. L. Scarf, W. Bernstein, R. W. Fredricks, *ibid.* **70**, 9 (1965).
7. L. A. Frank, J. A. Van Allen, H. K. Hills, *Science* **139**, 905 (1963).
8. J. A. Van Allen, private communication.
9. S. M. Krimigis and T. P. Armstrong, *Trans. Amer. Geophys. Union* **46**, 113 (1965).
10. L. A. Frank, J. A. Van Allen, E. Macagno, *J. Geophys. Res.* **68**, 3543 (1963).
11. J. A. Van Allen and S. M. Krimigis, *Trans. Amer. Geophys. Union* **46**, 532 (1965).
12. L. A. Frank, J. A. Van Allen, H. K. Hills, *J. Geophys. Res.* **69**, 2171 (1964).
13. J. R. Spreiter and W. P. Jones, *ibid.* **68**, 3555 (1963).
14. J. P. Heppner, N. F. Ness, C. S. Scearce, T. L. Skillman, *ibid.*, p. 1.
15. W. M. Elsasser, *Rev. Mod. Phys.* **22**, 1 (1950).
16. T. G. Cowling, *Magnetohydrodynamics* (Interscience, New York, 1957).
17. C. W. Allen, *Astrophysical Quantities* (Athlone Press, London, 1955).
18. P. M. S. Blackett, *Nature* **159**, 658 (1947).
19. ———, *Phil. Mag.* **40**, 125 (1949).
20. Development, construction, and preflight testing of the University of Iowa equipment on Mariner IV was supported by subcontract 950613 with the Jet Propulsion Laboratory. We thank T. P. Armstrong, D. L. Chinburg, and D. C. Enemark of the University of Iowa; and Dr. H. R. Anderson, R. K. Sloan, R. A. Lockhart, and D. Schofield of the Jet Propulsion Laboratory for help with various aspects of the work. The flight data used here are from the J.P.L. preliminary—though substantially complete—"users programs," which have been received promptly. Reduction and analysis of the data have been supported in part by NASA research grant NsG-233-62. S.M.K. and H.K.H. are graduate trainees of NASA.

12 August 1965

Search for Trapped Electrons and a Magnetic Moment at Mars by Mariner IV

Abstract. *The Mariner IV spacecraft on 14–15 July 1965 passed within 9850 kilometers of Mars, carrying a solid-state charged-particle telescope which could detect electrons greater than 40 kiloelectron volts and protons greater than 1 million electron volts. The trajectory could have passed through a bow shock, a transition region, and a magnetospheric boundary where particles could be stably trapped for a wide range of Martian magnetic moments. No evidence of charged-particle radiation was found in any of these regions. In view of these results, an upper limit is established for the Martian magnetic moment provided it is assumed that the same physical processes leading to acceleration and trapping of electrons in Earth's magnetic field would be found in a Martian magnetic field. On this basis, the upper limit for the Martian magnetic moment is 0.1 percent that of Earth for a wide range of postulated orientations with respect to the rotational axis of Mars. The implications of these results for the physical and biological environment of Mars are briefly discussed.*

Whether Mars has a general magnetic field—and consequently trapped radiation—is relevant to understanding the origin and evolution of Mars. Prior to this time there were no measurements of the magnetic fields or charged-particle radiation in the vicinity of the planet; hence any experiments which could detect a planetary field or charged-particle radiation are of intense physical and biological interest. The first opportunity to approach Mars came on 14–15 July 1965 when the Mariner IV spacecraft passed within 9850 km of the planetary surface. Two kinds of measurements were made which bear on the presence of planetary magnetic fields: namely, magnetometer observations (*1*) and charged-particle radiations of which we report here measurements from the University of Chicago instrument on the space probe.

To understand the relevance of charged-particle radiation to the existence of a planetary magnetic field we recall that the general field of Earth traps charged particles in radiation belts extending to the outer boundary between the geomagnetic field and the solar wind. Evidence now appears to be conclusive that, given these conditions, a planetary magnetic field will also lead to the buildup of locally accelerated particles within the magnetic field and that this trapped radiation will be present continuously, although the flux is highly variable in time. In addition, the supersonic solar wind and the interplanetary magnetic field which it contains interact with the magnetosphere to produce a bow shock at a characteristic stand-off distance beyond the magnetosphere (Fig. 1) (*2*). Associated with the bow shock are

bursts of electron fluxes found near the shock and beyond (Fig. 1, region 3) (*3*). Similar electron bursts are more densely distributed between the shock and the magnetospheric boundary (Fig. 1, region 2) (*4*). The trapped radiation distributed within the magnetospheric boundary constitutes a third electron region (Fig. 1, region 1). In what follows we assume that the same physical processes leading to acceleration and trapping of electrons in Earth's magnetic field would exist for any Martian dipole field. Thus there are three types of radiation "signatures," which could reveal the presence of a Martian magnetic field. Their relative locations would provide information on the magnitude of the Martian magnetic dipole moment.

We now report on a search for these three radiation signatures due to electrons greater than 40 kev—an energy range most likely, by analogy with Earth, to provide a sensitive test. The trajectory of Mariner IV provided a wide coverage of the possible charged-particle configurations around the planet. We find that there is no evidence for (i) a trapped radiation belt containing electrons greater than 40 kev energy, including electrons in the Mev energy range; (ii) electrons associated with a transition region between a bow shock and a magnetosphere; and (iii) electron spikes at a bow shock or at greater distances.

Normally, a planet with even a slight magnetic field might produce a wake extending in the antisolar direction from which some particle radiation might be expected to escape. The Mariner IV spacecraft did not pass through a possible Martian wake, but it did pass closely enough to have detected any substantial escape of electrons had such a wake existed. No effect was found.

If we introduce the simplifying assumption that the Martian magnetic field would be a dipole field, probably oriented in the direction of the spin axis of the planet, then we reach the following conclusions based on our observations:

1) There could not be a Martian dipole magnetic moment greater than

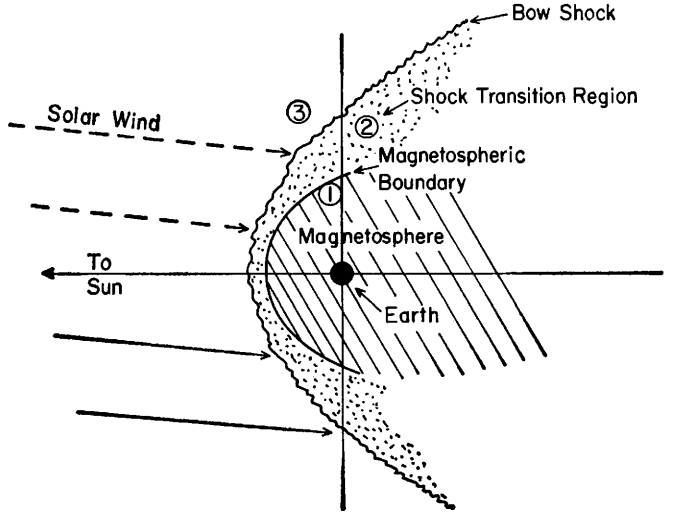

Fig. 1 (left). Relative location of electrons inside the magnetospheric boundary of Earth (*1*), the transition region (*2*), and outside the bow shock (*3*). The solar wind carries an interplanetary magnetic field of about 5×10^{-5} gauss.

Fig. 2 (below left). Cross-sectional view of charged-particle telescope. The main cone for particle acceptance is in the antisolar direction.

Fig. 3 (below). Calibrated response of the D_1 detector system for electrons. These curves are derived from laboratory measurements and take into account the aluminized-mylar window. The number of electrons required by pile-up to produce a count is given by the slope.

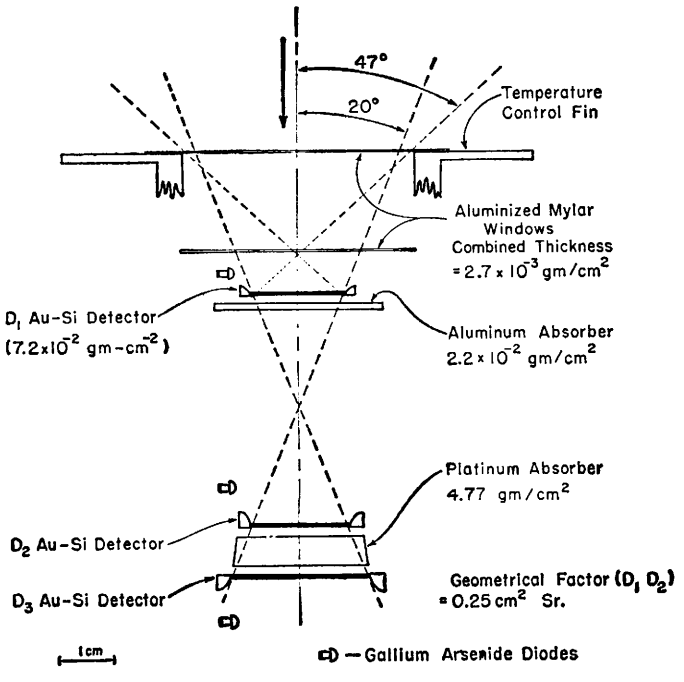

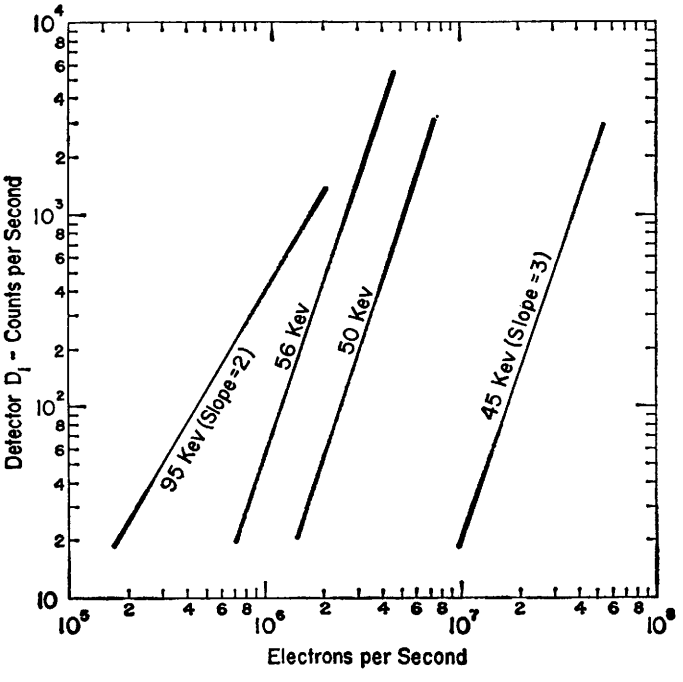

$2 \times 10^{-3} M_E$, where M_E is the present magnetic moment of Earth.

2) Since none of the three radiation signatures was observed it is very probable that the Martian dipole moment is substantially less than $10^{-3} M_E$.

These results have important implications for the physical and biological environment of Mars. For example, owing to the tenuous nature of the Martian atmosphere, as determined by the occultation experiment on board Mariner IV (*5*), the primary cosmic-ray flux reaches the entire surface of Mars; the generation of secondary particles through nuclear interactions takes place almost entirely below the surface of the solid planet.

The charged-particle telescope was designed to investigate charged-particle radiation in interplanetary space between the orbits of Earth and Mars and in the vicinity of Mars. The interplanetary experiments measured solar modulation of galactic proton and helium energy spectra and fluxes in the energy range 1 to 170 Mev per nucleon. Protons and helium nuclei from several solar flares, and 27-day recurring proton fluxes were studied. The instrument operated stably throughout the 228 days from launch to encounter with Mars and provided nearly continuous information over the entire period.

The following description of the instrument is limited to those characteristics of interest for the detection of charged particles near Mars. The telescope consists of three gold-silicon, surface-barrier detectors with aluminum and platinum absorbers as shown in the cross-sectional view of Fig. 2. The circular detectors, D_1 and D_2, have surface areas of 2.4 cm^2. The area of detector D_3 is 5 cm^2. Each detector has a silicon thickness of 500 μ, including a depletion depth (sensitive region) of 200 μ. Detectors D_1 and D_2 define an acceptance-cone angle of 40° for arriving charged particles. The geometrical factor for the arrival of low-energy particles at detector D_1 is 4 cm^2 sterad as determined by the geometry of the temperature control fin.

The axis of the acceptance-cone angle for charged particles is aligned with respect to the spacecraft so that it is always pointing away from the sun. The counting rates of charged particles fall into three intervals of particle energy. These energy intervals are determined by coincidence techniques. For example, particles which initiate pulses in D_1 but not in D_2 are designated $D_1\bar{D}_2$ events (including protons of 1 to ~15 Mev and electrons with energies as described below); particles which trigger both detectors D_1 and D_2 but not D_3 are designated $D_1D_2\bar{D}_3$ events; and so on. The number

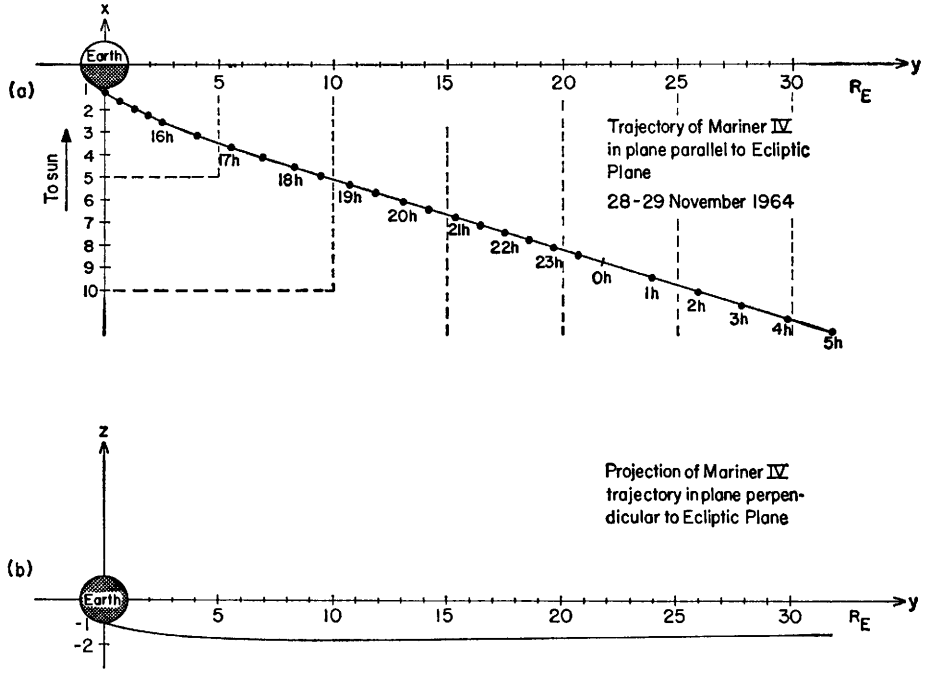

Fig. 4. The trajectory of Mariner IV away from Earth after launch, 28 November 1964. The coordinates are in units of Earth radii, R_E.

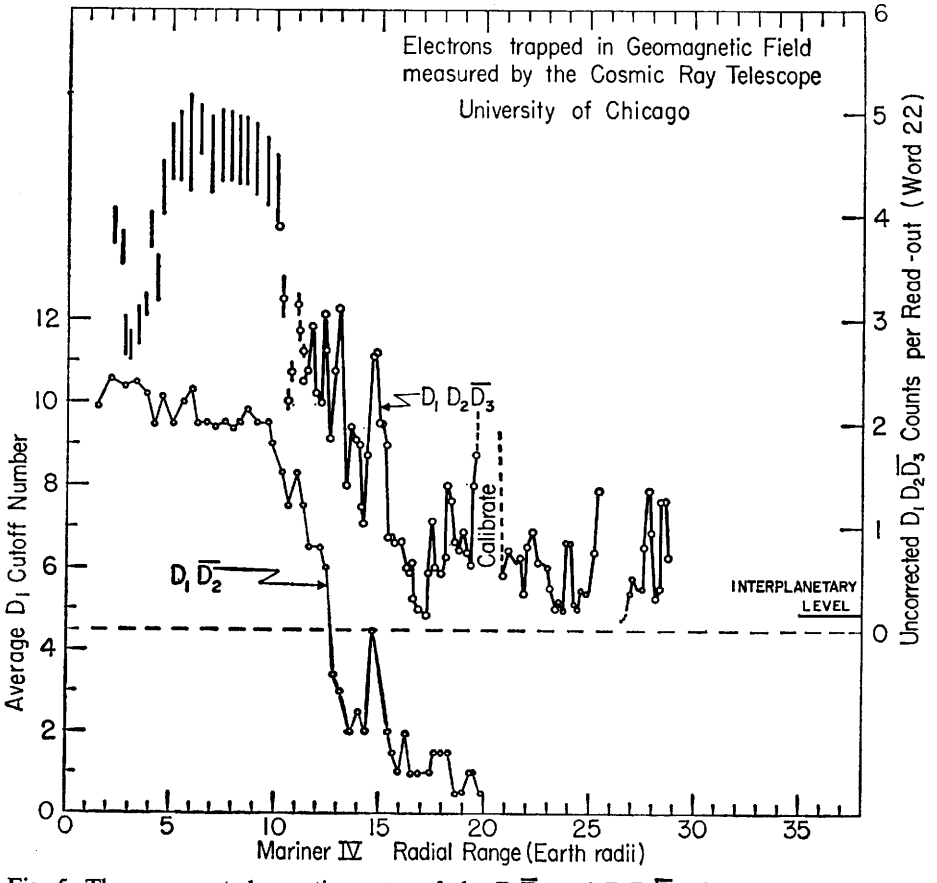

Fig. 5. The uncorrected counting rates of the $D_1\bar{D}_2$ and $D_1D_2\bar{D}_3$ channels for electrons in the geomagnetic field of Earth. For example, the peak at 18 R_E corresponds to about 400 count/sec for channel $D_1\bar{D}_2$.

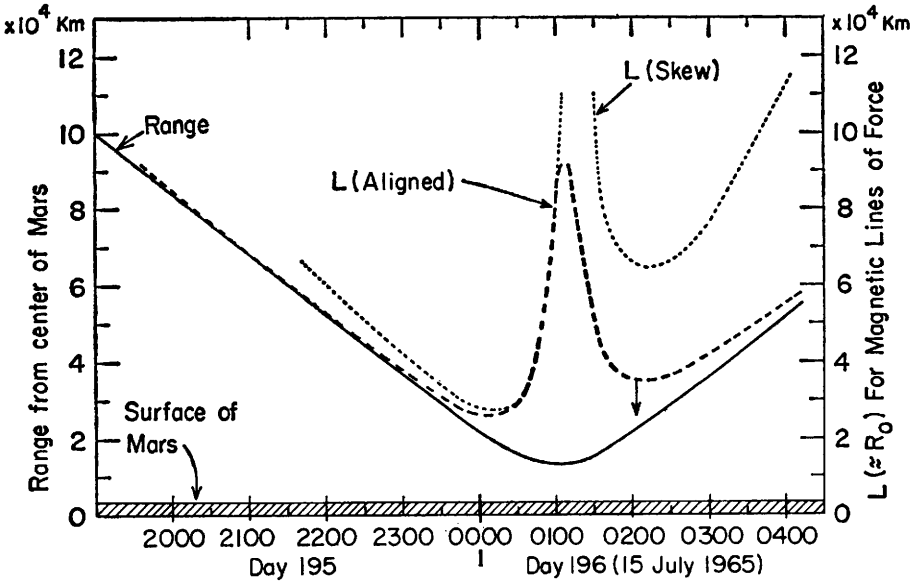

Fig. 6. Ordinate on left is the areocentric range of Mariner IV. Ordinate on right is equivalent to the equatorial radius of the line of magnetic force passing through the Mariner IV trajectory. Compression of the magnetic field by the solar wind lowers the second lobes of the "L" curves as shown by the arrow. Hours are in spacecraft time.

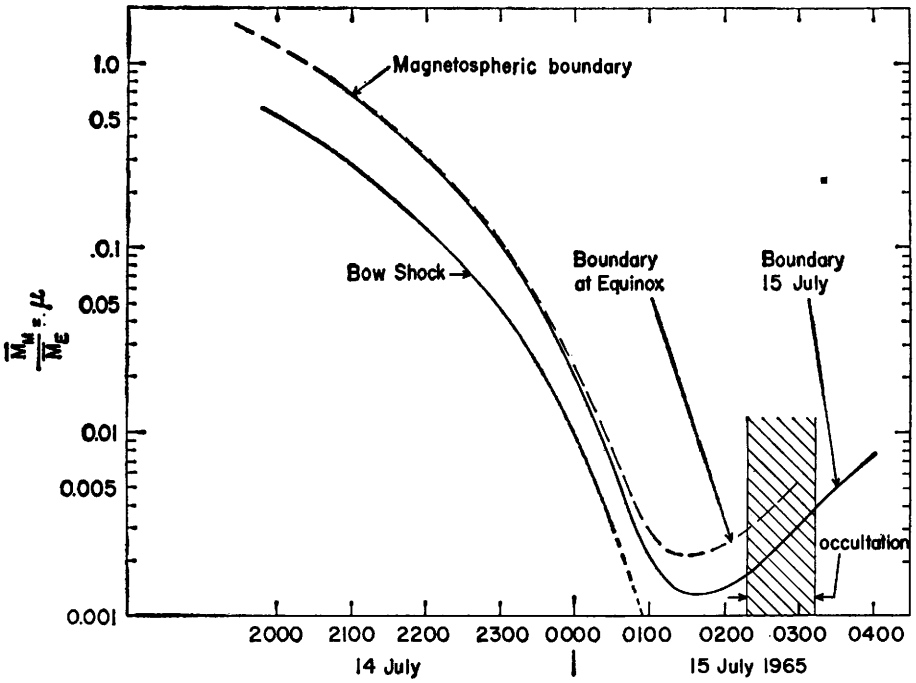

Fig. 7. Sensitivity for detection of Martian magnetic moment during encounter: M_M, Martian magnetic moment; M_E, Earth magnetic moment. On 15 July 1965 the arrival of the solar wind is 15° north of the Martian equator.

of events recorded in each of the three particle-range channels is read out periodically by the spacecraft data and telemetry systems. In addition, a 128-channel pulse-height analyzer in the instrument determines the pulse height in detector D_1 for the two higher particle-range intervals. The unique separation of protons from helium nuclei by this "energy loss and range" technique will not be described here. The complete instrument weighs 1.2 kg and requires 0.6 watt of power. The average information-bit rate for this experiment is 0.4 bit/sec. At periodic intervals the instrument is switched into a "calibrate" mode in order to check the performance of individual detectors.

Electrons are detected by the D_1 detector and the D_1D_2 detectors in coincidence. The aluminized-mylar window in front of the telescope established a low-energy limit of 40 kev for electron penetration. Above ~210 kev and up to several Mev energy, individual electrons are detected by D_1 with an efficiency exceeding 0.2. Below 210 kev electrons will be detected if the flux is high enough so that more than one electron arrives at the detector within the resolving time of the detector system. For electrons below ~100 kev we must also take into account both the energy dependence of electron transmission through the window (*6*), and the r.m.s. (root mean square) noise level of about 30 kev for the detector system. The response of a similar D_1 detector on the IMP I satellite to electrons in the vicinity of Earth's bow shock has been investigated (*3*) and a detailed investigation confirmed by laboratory electron accelerator studies is in preparation (*7*). The Mariner IV detector D_1 was identical with the IMP I detector except for its cross-sectional area and increased window thickness. In Fig. 3 we show the response curves calcu-

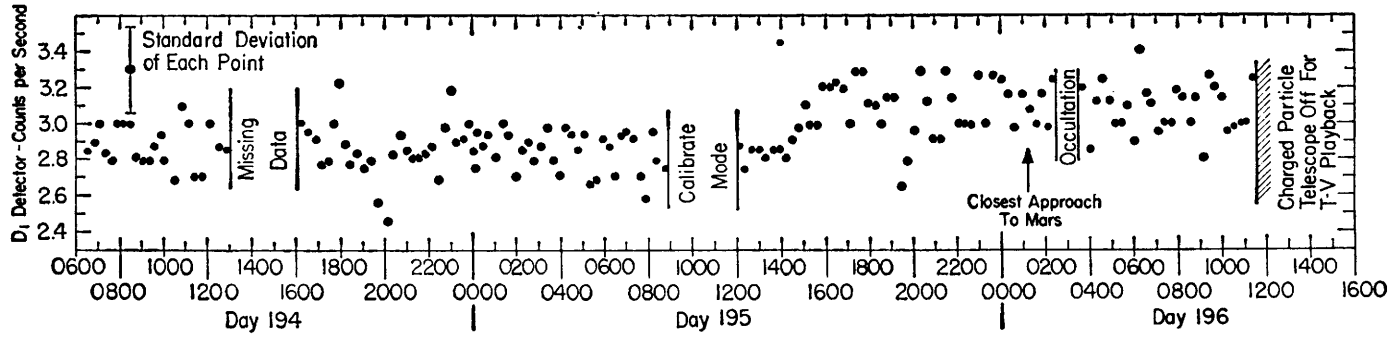

Fig. 8. Counting rates from the D_1 detector as a function of universal time. A small flux of low-energy interplanetary protons arrived at about 1500 U.T.

lated for the Mariner IV detector from the measured IMP I response.

As an example of the response of $D_1\bar{D}_2$ and $D_1D_2\bar{D}_3$ detector systems for electrons trapped within the geomagnetic field, we have obtained the data from the passage of Mariner IV through the geomagnetic field after launch on 28 November 1964. The trajectory projected in the plane of the ecliptic is shown in Fig. 4 where, by comparison with Fig. 1, we see that the trajectory passed the magnetospheric boundary at about 120° with respect to the Sun-Earth line and passed through the "dawn" side of the transition region behind Earth's bow shock. The electron data for the $D_1\bar{D}_2$ and $D_1D_2\bar{D}_3$ counting rate channels are shown in Fig. 5, not corrected for absolute flux levels. The instrument reaches saturation in the center of the outer Van Allen belt which extends (Fig. 5) out to approximately 10 R_E (units of Earth radii), but at greater distances the spatial and temporal structure of electron fluxes becomes clear. Typical electron "spikes" are observed in the transition region out to about 28 R_E. We note that on several occasions the counting rate between electron spikes in the transition region dropped to the interplanetary level in agreement with observations on IMP I (*3*).

With the knowledge of both the electron response of the telescope and the trajectory of the spacecraft relative to the planet Mars, we next explore the expected locations of characteristic electron signatures at Mars for a range of assumptions regarding the magnetic moment of Mars.

Models for Magnetic Fields and Particle Distributions. Not knowing the strength or orientation of a possible magnetic moment for Mars our objective is to examine the penetration of the Mariner IV trajectory into a wide range of possible model fields. In the discussion which follows we assume a magnetic dipole moment $\mathbf{M}_M$ located at the center of Mars. Our first task is to find the dipole lines of force which intersect the position of our detector as it passes through the assumed field. The identification of the lines of force on which a group of particles is moving is most conveniently specified (*8*) by a parameter L which, for a pure dipole, is equivalent to the equatorial radial distance R_0 from the dipole to the line of force on which the measurement is being made. For example, if the Mariner IV trajectory was confined to the equatorial plane of the dipole, the spacecraft range and the L-value for the magnetic line of force intersecting the spacecraft would be identical. However, since the spacecraft trajectory does not lie in the equatorial plane, the spacecraft range and the L-values are different. Electrons are most stably trapped in regions of small L-value. Clearly the minimum L-values reached during the traversal of Mars provide the most sensitive test for trapped radiation. In general this does not turn out to be the point of closest approach to the planet. The spacecraft trajectory passes from +10° to −68° magnetic latitude in its traversal of Mars. For the case $\mathbf{M}_M \parallel \bar{\omega}_M$ where $\bar{\omega}_M$ is the spin axis vector for Mars, the equatorial equivalent range of lines of force intersecting the spacecraft as a function of spacecraft time (*9*) is shown by the dashed line in Fig. 6, if there is no compression by the solar wind (*10*). In Fig. 6 the minimum L-values occur near 0020 hour and 0200 hour, spacecraft time. To approximate the "worst case" we have tilted $\mathbf{M}_M$ by 40° in the plane which includes $\bar{\omega}_M$ and the spacecraft at 0110 hour, as represented by the dotted line for L (skew) in Fig. 6.

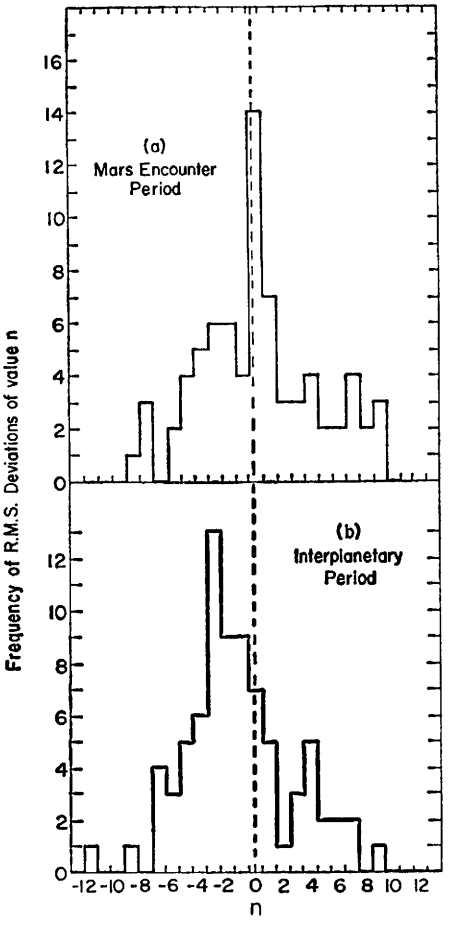

Fig. 9. *a*, 22 hours of data centered on time of closest approach to Mars; *b*, 24 hours of interplanetary data before "calibrate."

If now we introduce the solar-wind compression of the magnetic field on the sunward side as shown in Fig. 1 for Earth, the lines of force become distorted. This has the effect of lowering the second lobes of the L-value curves relative to the first lobes as indicated by the arrow in Fig. 6. Approximate solutions are not yet available for L-values from a compressed dipole field of arbitrary orientation with respect to the solar wind. The above considerations are independent of the value of $\mathbf{M}_M$.

Studies of the Earth's magnetosphere have shown that the location of the magnetospheric boundary is determined by a balance between the solar-wind pressure and that of the magnetic field; theoretical treatments for the cases of $\mathbf{M}$ perpendicular (*11*) and parallel (*12*) to the solar wind have served as a basis for our discussion. We extrapolated the measured density of the solar wind at Earth to Mars using the fact that it varies as the inverse square of the distance from the Sun. Furthermore the magnetospheric radius scales as the $-\frac{1}{6}$ power of the solar wind pressure. Thus if we call $R_{mag\text{-}M}$ and $R_{mag\text{-}E}$ the radial distance of the magnetospheric boundary at Mars and Earth respectively we obtain the approximate scaling law

$$R_{mag\text{-}M} = 1.16 \left(\frac{M_M}{M_E}\right)^{\frac{1}{3}} R_{mag\text{-}E}$$

In the following discussion we let $\mu = M_M/M_E$. With the given trajectory for Mariner IV we then obtain μ as an implicit function of the time at which Mariner IV crosses a Martian magnetospheric boundary over the range $\mu = 10^0$ to 10^{-3} as shown in Fig. 7 for $\mathbf{M}_M \parallel \bar{\omega}_M$. For small values of μ the magnetic latitude of incidence for the solar wind becomes important. This angle was 15° on 15 July 1965, and it lowers by a factor of 2 the detection range of $\mathbf{M}_M$ by Mariner IV.

From Fig. 7 and the lowering of the second lobe in Fig. 6, we conclude that the most sensitive time interval for the detection of trapped radiation along the Mariner IV trajectory lies between about 0140 hour and occultation.

The distance of the bow shock

Some Planetary and Orbital Characteristics of Mars*

Mean distance from Sun	227.94×10^6 km
Inclination of orbit from ecliptic plane	1° 51′
Inclination of equator from orbital plane	23° 59′
Eccentricity of orbit	0.093
Period of revolution about Sun	686.98 days
Period of rotation about axis	24 hours, 37 minutes
Equatorial radius	3380 km (0.53 times Earth radius)
Mass	0.108 times mass of Earth
Mean density	3.97 gm/cm³
Surface acceleration due to gravity	376 gm/sec²

* All values are from C. W. Allen, *Astrophysical Quantities* (Athlone Press, London, ed. 2, 1963).

R_b from the dipole is estimated in analogy with the observed conditions at Earth. If we take $R_{mag\text{-}M}$ along the Sun-Mars line, we assume $R_b = KR_{mag\text{-}M}$, with $K = 1.3$ for the shock stand-off distance. Figure 7 gives μ as a function of the time of passage through the shock. The results are uncertain for very small values of μ as shown by the dashed extension of the bow-shock curve.

We now apply the above considerations to the search for trapped radiation by making the assumption that the fundamental mechanism for particle acceleration and trapping observed in the earth's magnetosphere will scale down continuously over a reduction of more than 10^3 in equivalent magnetic moment. We note that before and during the measurements at Mars the interplanetary conditions were generally quiescent (*13*) with no significant magnetic storms which could have "dumped" the radiation which might be present. Therefore, the particle energy density U in the magnetic field B at Mars would be expected to rise to a value $U = A(B^2/8\pi)$, where A is less than 0.1 for electron energies more than 40 kev.

The boundary of the magnetosphere is determined by the balance of magnetic-field pressure and the solar-wind pressure: when the Sun-Mars-probe angle is large this field strength may lie in the range 20 to 80×10^{-5} gauss. Thus, inside but near the boundary we expect the omnidirectional electron flux to be of the order 10^4 to 10^5 electrons per square centimeter (for example, see the IMP I measurements with a detector similar to D_1, ref. *7*). Assuming an integral spectrum proportional to E^{-3} (E = kinetic energy) and the response of D_1 given by Fig. 3, we calculate that the expected counting rates for D_1 will be of the order 50 count/sec over the entire range of μ in Fig 7 *at the boundary*. By assuming a spectrum proportional to E^{-2} from the recent observations of Frank (*14*), our D_1 counting rate would be approximately 2000 count/sec. Substantial penetration inside the boundary to the minimum L-values for a given μ will further increase the flux levels by at least an order of magnitude. The above estimates take into account the fact that the traversal of minimum L-values for the magnetic field occurs at −50° to −30° magnetic latitude.

Since an increase of 0.7 count/sec could be detected in D_1 with 99-percent confidence when averaged over a single period of 16.7 minutes (equal to ten successive readouts of the telemetry word) we see that any crossing of a magnetospheric boundary would be detected. Additional flux enhancements would be observed inside the magnetosphere.

Observations at Mars. The D_1 counting rate was averaged for successive 16.7-minute intervals within which there were ten samples of approximately 0.3 minutes each. These data are presented in spacecraft time sequence in Fig. 8. It is apparent that the counting rate increased slightly and began fluctuating at about 1500 hour, 1.7×10^5 km away from the planet. The available evidence at present is against this increase in counting rate being associated with the planet. First, several small proton events have been observed by the charged-particle telescope in interplanetary space, especially within the 2-month period preceding encounter with Mars. Second, there seems to be no reasonable way in which this radiation could be associated with the planet, extend out to 1.7×10^5 km, and continue at roughly *the same level* until the end of transmission at 1148 hour on 15 July. For these reasons we assign a solar or interplanetary origin to this proton flux.

In Fig. 9 we compare the frequency of r.m.s. deviations about the means for (*a*) the Mars encounter period and (*b*) the interplanetary medium. There are no statistically significant differences in these distributions. These

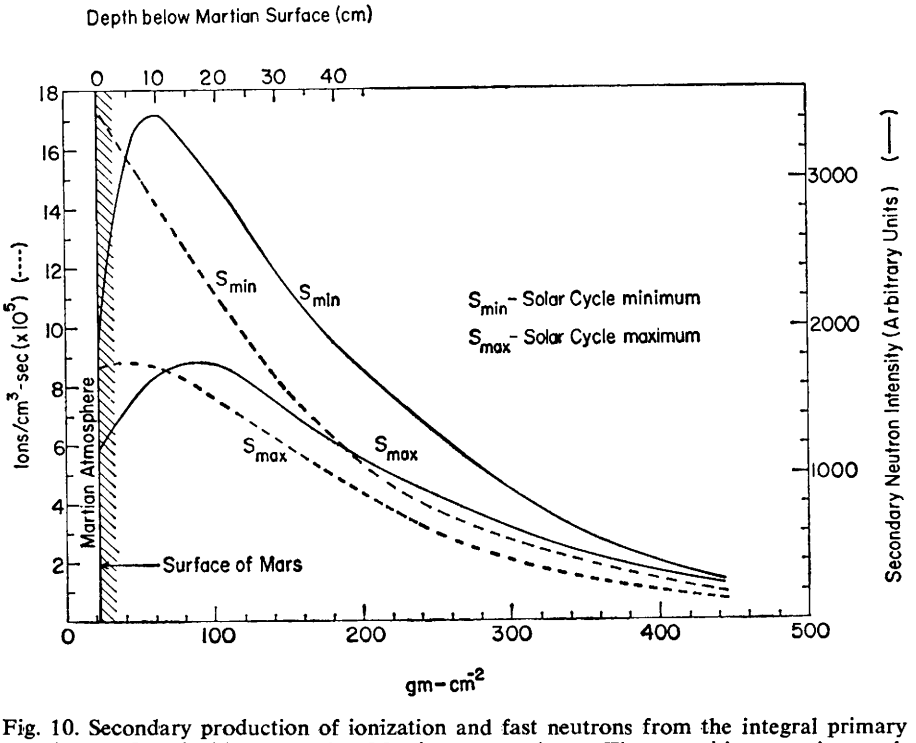

Fig. 10. Secondary production of ionization and fast neutrons from the integral primary cosmic-ray flux incident on the Martian atmosphere. The transition maximum is underground.

curves are similar to other interplanetary distributions studied in earlier months. We conclude with 99-percent confidence that no increase in counting rate greater than or equal to 1 count/sec was observed which could be associated with Mars. In view of the expected counting rates for a signature arising from a magnetospheric particle flux discussed above we conclude that the absence of this signature alone establishes an upper limit of $\mu \leq 2 \times 10^{-3}$.

A similar investigation of the $D_1D_2\bar{D}_3$ counting rate and the pulse-height distribution of analyzed events also revealed no additional particles associated with the planet.

Turning our attention to the transition region, we recall that multiple electron spikes are expected, similar to the case at Earth in Fig. 5 for $R > 13R_E$. For small values of μ, the shock and transition regions would be entered by Mariner IV towards the "evening side." It has been found (*15*) that there are fewer electron spikes in the transition region on the evening side than on the dawn side. There is approximately a 20-percent probability of seeing a single electron spike; if there are about ten of them, a substantial increase of intensity should have been observed with a probability of about 90 percent. No increase was observed.

Finally, if a bow shock existed, due to the presence of a magnetosphere, electron spikes will be found frequently beyond the shock (*3*). For this case the probability of our observing particles is about 50 percent. No radiation was detected.

From the above discussion we find that the upper limit of μ may be further reduced to $\mu \leq 10^{-3}$. Since the location of a magnetospheric boundary is not strongly dependent on the orientation of $\mathbf{M}_M$, we believe this result applies to almost all orientations of $\mathbf{M}_M$.

Mariner IV passed outside of, but near, any planetary wake which might have existed. However, if such a wake existed, particles might escape to the nearby planetary medium. We observed no evidence of additional particles.

We have searched and found no evidence for charged-particle radiation associated with Mars. In view of the close approach of the Mariner IV trajectory to Mars, we are able to set an upper limit to its magnetic moment provided we assume that the same physical processes leading to acceleration and trapping of electrons in Earth's magnetic field would be found in a Martian magnetic field. We find that the magnetic moment of Mars is less than 10^{-3} that of Earth for a wide range of postulated orientations with respect to the rotation axis of Mars.

These conclusions lead to several implications bearing on the probable physical and biological conditions on the planet, some of which are:

1) The full intensity of cosmic radiation and solar flare protons in the vicinity of Mars will reach the top of the Martian atmosphere over the entire planet. Since observations by Mariner IV have shown (*5*) that this atmosphere is only about 10 g/cm^2, virtually the entire secondary production of particles from high-energy interactions takes place *below* the surface of Mars instead of in the atmosphere as at Earth. In Fig. 10 we have estimated the distribution of ionization (left-hand ordinate) and fast neutrons (right-hand ordinate) from the cosmic radiation using data obtained from measurements at Earth (*16*) and assuming that the surface density of the planet is its mean density, 3.97 g/cm^3. Solar-flare protons in excess of 100-Mev energy will also penetrate to the surface. It is important to note that a large fraction of the energy from cosmic ray interactions goes into π-meson production. Since these π-mesons are produced in the solid planet they will interact with nuclei below the Martian surface, instead of decaying to μ-mesons as they would in Earth's atmosphere. Consequently, secondary neutron and proton production in the solid planet considerably exceeds the production found at Earth. Thus, the production of radioactive and stable isotopes will be concentrated under the Martian surface. Since the density of Moon is 3.34 g/cm^3 we might expect that the secondary neutron flux escaping from Mars and Moon would be comparable.

2) It may be argued that a negligible magnetic moment for Mars means that it has no liquid iron-nickel core within which circulating current systems could be established. This may be correct, but it is not certain, since there are a variety of ways—suggested by studies of paleomagnetism—in which the internal motions may be slow and changing in character. However, the interior planetary conditions are not likely to be similar to Earth's.

3) If, in fact, a general Martian magnetic field is nonexistent the solar-wind protons are continually interacting with the Martian atmosphere. It is not yet clear from the competing effects of capture processes and escape of molecules through collisions whether or not the atmosphere has a lifetime comparable to the age of the planet. Perhaps Mars will have a "tail" of streaming molecules and ions whose origin is the Martian atmosphere.

J. J. O'GALLAGHER
J. A. SIMPSON
Enrico Fermi Institute for Nuclear Studies and Department of Physics, University of Chicago, Chicago, Illinois

References and Notes

1. E. J. Smith, L. Davis, Jr., P. J. Coleman, Jr., D. E. Jones, *Science*, this issue.
2. N. F. Ness, C. S. Scearce, J. B. Seek, *J. Geophys. Res.* **69**, 3531 (1964), and references therein.
3. C. Y. Fan, G. Gloeckler, J. A. Simpson, *Phys. Rev. Letters* **13**, 149 (1964).
4. L. A. Frank, J. A. Van Allen and E. Macagno, *J. Geophys. Res.* **68**, 3043 (1963).
5. A. J. Kliore, D. L. Cain, G. S. Levy, V. R. Eshelman, F. Drake, *Science*, this issue.
6. R. Arnoult, *Ann. Phys. Ser. 11* **12**, 241 (1939).
7. C. Y. Fan, G. Gloeckler, J. A. Simpson, preprint, Enrico Fermi Institute for Nuclear Studies, 65-66, in press.
8. C. E. McIlwain, *J. Geophys. Res.* **66**, 3681, 1961.
9. Since the time for radio signals to travel from the spacecraft to Earth is 12 minutes, spacecraft time and Universal Time differ by approximately 12 minutes.
10. H. R. Anderson, J.P.L. interoffice memorandum, 3 May 1965.
11. G. D. Mead and D. B. Beard, *J. Geophys. Res.* **69**, 1169 (1964).
12. R. Blum, *Phys. Fluids*, in press.
13. Nat. Bur. Std. Central Radio Propagation Laboratory, Boulder, Colo., Rept. Ser. B, July 1965.
14. L. A. Frank, *J. Geophys. Res.* **70**, 1593 (1965), and references therein.
15. M. D. Montgomery, S. Singer, J. P. Conner, E. E. Stogsdill, *Phys. Rev. Letters* **14**, 209, 1965.
16. H. V. Neher, *Semaine d'Etude sur le Probleme du Rayonnement Cosmique dans l'Espace Interplanetaire* (Vatican City, Rome, 1963), p. 281; J. A. Simpson, in *Science in Space*, L. Berkner and H. Odishaw, Eds. (McGraw-Hill, New York, 1961), p. 266.
17. We thank R. Jacquet, R. Weissman, R. Takaki, and the staff of our Laboratory for Astrophysics and Space Research for the electronic design, engineeering, and fabrication of the flight and test instruments. A. Tuzzolino, J. Kristoff, and P. Shen provided the excellent detectors. S. Myles assisted in the programming and data reduction. For the preparations and calculations concerned with encounter we appreciate the assistance of J. Sullivan and R. Blum. Both R. Holman and H. Anderson of the Jet Propulsion Laboratory gave us assistance and advice throughout the mission for which we are grateful. We also thank the J.P.L. Mariner-C staff for integration of our experiment into the spacecraft and for accomplishing a difficult mission. Assisted in part by NASA grant NSG 179-61 and contract NASA-JPL-950615; and by Air Force OSR grant 521-65. J.O'G. is a NASA predoctoral fellow.

16 August 1965

Zodiacal Dust: Measurements by Mariner IV

Abstract. *Data from the Mariner IV dust-particle experiment reveal an increase by a factor of 5 in the flux of interplanetary dust particles as the heliocentric distance from the sun increases. There is a variation in the slope of the cumulative flux-mass distribution, with the steepest slope for the distribution occurring between the planets. No enhancement of the flux in the vicinity of Mars was detected.*

The objective of the cosmic-dust experiment on Mariner IV was the measurement of the mass and flux distributions of interplanetary dust particles in the vicinity of the earth, between the orbits of the earth and Mars, and in the vicinity of Mars. Prior to the Mariner IV mission, the primary information concerning these dust particle distributions had been obtained from analysis of photometric studies of the zodiacal light, solar corona, gegenschein (counterglow), and the cosmic-dust experiment on Mariner II (*1*). The major features of the measurements from the cosmic-dust experiment on Mariner IV are: (i) an enhancement of the flux as the heliocentric distance from the sun increases; (ii) a change in the cumulative flux-mass distribution curve with the flux varying as a function of $m^{-0.55}$ (m, mass) near both planets to $m^{-0.9}$ between the planets; (iii) no statistically significant evidence of any well-defined dust particle streams; (iv) no measurable enhancement of the flux in the vicinity of Mars; and (v) the flux measured by the Mariner II experiment is consistent with the measurements from the Mariner IV instrumentation near 1 AU, which indicates that the flux, between 0.72 AU and 1.2 AU is fairly constant.

The experiment detector consisted of an aluminum sensor plate (area = 3.5×10^{-2} m^2) with an acoustical transducer bonded to this plate. In addition, a thin film capacitor covered each side of the plate providing another detector sensitive to high speed microparticle impacts. The impact plate was mounted in such a manner that each side of this sensor was exposed to cosmic dust impacts. The acoustical transducer produces a signal related to the mechanical impulse received by the sensor plate from a dust particle impacting on either side of the plate. The capacitor sensors detected the side of the plate on which an impact occurred. The electronic instrumentation contained a storage system which accumulated all dust-particle impacts and provided eight levels of pulse-height analysis to the signal from the acoustical transducer. This system also provided information concerning the occurrence of coincidences between signals from the acoustical transducer and the capacitor sensors. The threshold sensitivity of the acoustical transducer was $6 \pm 0.7 \times 10^{-5}$ dyne-sec. The dynamic range of the pulse-height analyzer extended to 1.96×10^{-3} dyne-sec. The system simply counted particles for which the momenta were larger than 1.96×10^{-3} dyne-sec. The instrumentation also contained an experiment calibration which was performed approximately three times a day when the telemetry was on the high bit rate, and approximately once a day when the telemetry was on the low bit rate. The viewing solid angle of the system was approximately π steradians.

The measurements reported here cover the period of time which starts at approximately 10 hours after launch (0000 U.T., 29 November 1964) and goes through the encounter with Mars (approximately 0100 U.T., 15 July 1965). All in-flight calibrations of the experiment instrumentation were proper in all respects. Of the 215 impacts recorded, 18 occurred during times when, for various reasons, the telemetry stations were not receiving transmission from the spacecraft. The experiment accumulator recorded these events, but no pulse-height analysis information was available. Pulse-height analysis information was obtained for the remaining 197 impacts.

The preliminary data are presented in Table 1. Between 1 and 1.25 AU, the cumulative flux was 7.3×10^{-5} particle m^{-2} sec^{-1} (π steradian)$^{-1}$. As the distance of the spacecraft from the sun increased, the measured flux also increased and reached a peak of 3.3×10^{-5} particles m^{-2} sec^{-1} (π steradian)$^{-1}$ between 1.36 and 1.43 AU. The flux then decreased to 1.8×10^{-4} particle m^{-2} sec^{-1} (π steradian)$^{-1}$ at encounter with Mars. From the data in Table 1, the measurement indicates a flux enhancement of a factor of 5 as the heliocentric distance from the sun increased. The maximum flux occurred at a heliocentric distance roughly equal to the perihelion distance of Mars (1.38 AU).

Table 1. Cumulative flux-mass distribution for various heliocentric distances. N_p, number of impacts; Δt, time in days with first data interval starting at 0000 U.T., 29 November 1964, and last interval ending at 0100 U.T., 15 July 1965; psd, probe-sun distance in AU for each data interval; Φ, mean cumulative flux for each data interval in particles m^{-2} sec^{-1} (π steradian)$^{-1}$; β, slope of cumulative mass distribution.

N_p	Δt (days)	psd (AU)	Φ	β
44	100	1.0 –1.25	7.3×10^{-5}	−0.5
43	34	1.25–1.36	2.1×10^{-4}	−0.9
40	20	1.36–1.43	3.3×10^{-4}	−0.6
39	29	1.43–1.49	2.2×10^{-4}	−0.55
49	45	1.49–1.56	1.8×10^{-4}	−0.6

The cumulative flux for each interval listed in Table 1 can be related to particle mass by an expression of the form: $\Phi \alpha m^{\beta}$. The values of β for the intervals shown in Table 1 demonstrate the variation of the flux-mass distributions between 1 and 1.56 AU. With one exception, the value of β generally varies between −0.5 and −0.6. The exception to this value of β is in the second interval in Table 1, for which a value of −0.9 was obtained. In general, the value of β for the flux-mass distribution is the same in the general region of the two planets, but a steeper slope of the distribution was measured between the planets.

A comparison can be made between the flux indicated by the Mariner II measurement where two impacts were recorded. The flux and mass distributions for the first interval in Table 1 indicate that 3 ± 2 impacts could be expected from the Mariner II measurement. Since the Mariner II result is consistent with the data from the first interval of the Mariner IV measurement, the flux and mass distributions between 0.72 and 1.25 AU may be similar.

The Mariner IV experiment provides the first opportunity to compare direct measurements of flux-mass distributions of dust in the zodiacal cloud with those made with ground-based photometric instruments. Previous analyses (*2*) have come from satellite measurements of flux-mass distributions in the vicinity of the earth. In general, the flux-mass distributions obtained from the ground-based observations contain β approximately equal to −0.5 when large (10 to 100 μ in diameter) particles are assumed in the analysis. When analyses are made with the Mie theory of light

scattering by small dust particles, steeper slopes for flux-mass distributions are obtained with $\beta \approx -0.9 \pm 0.1$ for much smaller particles (1 to 10 μ diameter). In addition, most of the analyses of flux distributions based on ground-based observations follow the assumption that decrease of flux is a function of increasing heliocentric distance. The measurement from Mariner IV shows a variation in the flux-mass distribution with the steepest slope of the distribution occurring between the planets. The measurement also yields a flux which increases with heliocentric distance from the sun. Neither of these results have been included in the analyses of ground-based photometric observations.

The experiment has been resumed after the playback of the pictures of the planet, and data are being obtained. Additional information concerning the apparent enhancement of flux near the perihelion distance of Mars may be obtained whenever there are communications with the spacecraft.

W. M. ALEXANDER
C. W. MCCRACKEN
Goddard Space Flight Center, National Aeronautics and Space Administration, Greenbelt, Maryland

J. L. BOHN
Department of Physics, Temple University, Philadelphia, Pennsylvania

References

1. W. M. Alexander, *Science* **138**, 1098 (1962).
2. M. Dubin and C. W. McCracken, *Astronom. J.* **67**, 248 (1962).

16 August 1965

Magnetic Field Measurements near Mars

Abstract. *During the encounter between Mariner IV and Mars on 14–15 July, no magnetic effect that could be definitely associated with the planet was evident in the magnetometer data. This observation implies that the Martian magnetic dipole moment is, at most, 3×10^{-4} times that of the earth.*

This is a preliminary report of the magnetic field measurements that were made near Mars on 14–15 July by the Mariner IV magnetometer. No effects definitely attributable to the presence of the planet were observed. This conclusion is based on a comparison of the encounter data with the measurements recorded by the same instrument within the region of interaction between the earth's magnetic field and the solar wind, as well as in interplanetary space during the 7-month interval between launch and encounter. It is assumed that the interaction of the solar wind with a significant Martian dipole moment would have produced effects geometrically similar to those observed near the earth, but with a scale determined by the magnitude of the dipole moment. This assumption is used to establish an upper limit for the Martian dipole moment. Since the bow shock (*1*) is the feature of a planet's interaction with the solar wind that occurs farthest from the planet (except possibly for the magnetic tail, which we were never in a position to detect because of the nature of the trajectory), the ability to detect such a shock forms the basis for our discussion. The ability of the Mariner magnetometer to detect a planetary shock front depended on the spatial resolution and sensitivity of the measurements, on the character of the interplanetary field fluctuations during encounter, and on the nature of the encounter trajectory.

The resolution of the telemetered magnetic data was 0.35 gamma per axis (1 gamma = 10^{-5} gauss), a limit imposed by the uncertainty inherent in converting the magnetometer output analog signals to digital numbers before transmission to Earth. The noise threshold of the Mariner's vector helium magnetometer was significantly smaller, being equivalent to only 0.1 gamma rms per axis. Measurements were made in a 50.4-second cycle in which the intervals between consecutive simultaneous triaxial observations were 6.0, 3.6, 9.6, and 31.2 seconds after which the cycle repeated. During passage through the earth's bow shock, the sensitivity was the same, but each interval was only one quarter as long. Data obtained slightly behind the extended dawn line showed clear evidence of the geomagnetic bow shock as it repeatedly surged back and forth past the spacecraft (*2*). The region behind the shock front was characterized mainly by fluctuations about the mean with amplitudes of the order of 2 gamma and with prominent frequencies, as judged by the amount of change over the various lengths of the sampling intervals, of the general order of 0.1 cy/sec and lower. There were also changes of several gammas across the bow shock in the average components of the field. The bow shock around Mars should occur at a position where the field strength has a value determined by the solar-wind pressure (that is, its momentum flux), and hence the characteristics of the shock should be largely independent of the Martian magnetic moment and quite similar to what is observed at the earth.

Throughout the 7-month period in interplanetary space the Mariner magnetometer data show a pattern of alternating disturbed and quiet intervals which has come to be expected of these kinds of data and which is related to daily changes in solar activity. Fortunately the time interval before, and during, encounter was one of relative magnetic calm, even though the Mariner's energetic particle detectors were recording a solar proton event that began about 23 hours prior to encounter (*3*). During the interval from 1800 on 14 July to 0123 Universal Time, 22 minutes after closest approach, the field was unmistakably interplanetary in character, having fluctuations roughly an order of magnitude smaller than those behind the earth's bow shock. At 0123 U.T., a period of disturbance began abruptly with a 5-gamma jump in the field and an approximate doubling of the amplitude of the fluctuations. This condition continued for about 3 hours, after which the components returned to near their previous values. This disturbance could be interpreted as evidence for a weak bow shock associated with Mars, but our preliminary analysis does not exclude the possibility that it is just one of many similar disturbances seen in the 7-month period.

The Mariner flight path approached Mars from a direction 13° above the equatorial plane and at 0940 local time. It crossed the noon meridian at a latitude of −50° and an areocentric distance of 14,500 km or 4.3 r_M (Martian radii); it dipped down 21 minutes later to a latitude of −67° at closest approach, where the local time was 1435 and the areocentric distance 13,200 km or 3.9 r_M. Mariner did not pass into the shadow of the planet, but moved away in a direction making an angle with the Sun-Mars line of about

145°, the local time being 2150 and the latitude being −3°. Beginning at 0219 U.T. (about 1 hour after closest approach), Mariner IV was occulted by Mars for 54 minutes, and no telemetry data were received. However, this gap in the record does not significantly affect our estimate of the Martian dipole moment, since a moment large enough to cause a significant effect during this interval would have caused detectable effects before occultation.

Satellite and space probe measurements made near the earth must be scaled in order to make them applicable to a planet having a different dipole moment. We use essentially the same approach here that we applied to the Mariner II data obtained near Venus (*4*). We assume that the locations and shapes of the magnetopause and the shock front are approximate surfaces of revolution about the solar direction and are reasonably insensitive to orientations of the magnetic dipole. Then the dipole moment of Mars (M_M) can be expressed in terms of the earth's dipole moment (M_E), the typical solar wind pressure at earth (P_E), the actual wind pressure at the planet (P_M), the areocentric distance to a point on the encounter trajectory at which an effect such as the magnetopause or shock occurs (R_M), and the geocentric distance (R_E) to the corresponding feature near earth at the same sun-planet-spacecraft angle:

$$M_M/M_E = (R_M/R_E)^3 (P_M/P_E)^{\frac{1}{2}}$$

In this report, we use this equation to derive an upper limit for M_M from the observation that no magnetic disturbance was seen before 0123 U.T. when Mariner was 14,700 km from the center of Mars at a Sun-Mars-spacecraft angle of 110°. Near Earth at a Sun-Earth-spacecraft angle of 110°, the Mariner IV data showed that the position of the shock front varied between 233,000 and 246,000 km at a time when the velocity of the solar wind was 400 km sec^{-1} and the density was about 6 cm^{-3} (*5*). These data, when combined with the IMP-1 (interplanetary monitoring platform) shock front data (*6*), lead to a reasonable, smooth contour for the average shock front location.

The typical value for R_E at an angle of 110° is 240,000 km (~37.5 r_E). Average values for the solar wind parameters during the IMP-1 observations (8 cm^{-3} and 340 km sec^{-1}) (*5*) correspond to an average pressure (P_E) of 2.10^{-8} dyne cm^{-2} in good agreement with the above Mariner IV plasma measurements. During encounter, the preliminary values for the velocity and density of the solar wind are 330 km sec^{-1} and 2 cm^{-3} (*5*), respectively, so that P_M is approximately 0.5×10^{-8} dyne cm^{-2}. Substituting these values into the equation above gives $M_M \leq 10^{-4} M_E$. These results could be changed somewhat if allowance were made for the possibility that the dipole axis of Mars may not be parallel to the rotation axis and for the fact that the earth's bow shock has not been completely explored and will deviate somewhat from a surface of revolution. However, we are confident that the maximum uncertainty is a factor of 3 and that the upper limit to M_M lies between 3×10^{-4} and 10^{-4} M_E.

If the disturbance that started at 0123 U.T. is regarded as interplanetary because the amplitude of the fluctuations appears to resemble other interplanetary disturbances more than the earth's bow shock, the actual value of M_M must be smaller than the upper limit given above, and it may well be zero. If the disturbance is regarded as a weak bow shock, then the above values should be regarded as giving the range within which the actual magnetic moment of Mars must lie.

Some of the consequences of this small upper limit for M_M are immediately apparent. Any field-producing dynamo must be nearly inactive. Since the rotation rates of Mars and the earth are nearly the same, a very small fluid core is suggested for Mars, in agreement with earlier proposals (*7*). The Martian interior now appears definitely to be more like the interior of the moon than that of the earth. A moment of 3×10^{-4} M_E implies a surface field at the magnetic equator of only 100 gamma. It also means that the flux of cosmic rays above the atmosphere should everywhere be comparable to what is observed at earth only over the polar regions. The elevation of the magnetopause in the subsolar region is, at most, 5000 km or 1.5 r_M. The very weak fields and low L value for the magnetopause imply that any belts of trapped radiation on Mars must be very small and weak. If the dipole moment is zero, there can be no trapped radiation.

If there is no intrinsic dipole moment due to interior sources, the solar wind, with its embedded interplanetary magnetic field, must press in against the Martian atmosphere to the level at which the ion pressure balances the stagnation pressure of the solar wind. The energy and momentum fluxes of the solar wind are large enough that if they interact with the Martian atmosphere at this level with moderate efficiency, they will remove it at a rate that is significant in any treatment of its evolution. As suggested by Gold (*8*) with regard to the moon, some of the interplanetary field lines should diffuse into Mars. The field lines will tend to pile up at the subsolar point and to be swept around the planet by the solar wind. It seems probable that in this case there would be a weak bow shock outside the stagnation region; and it may be that the disturbance seen at 0123 is associated with this tentative model (*9*).

EDWARD J. SMITH
Jet Propulsion Laboratory, Pasadena, California

LEVERETT DAVIS, JR.
California Institute of Technology, Pasadena

PAUL J. COLEMAN, JR.
Institute of Geophysics and Planetary Physics, University of California, Los Angeles

DOUGLAS E. JONES
Brigham Young University, Provo, Utah

References and Notes

1. W. I. Axford, *J. Geophys. Res.* **67**, 3791, (1962); P. J. Kellogg, *ibid.*, p. 3805; J. R. Spreiter and W. P. Jones, *ibid.* **68**, 3555 (1963).
2. P. J. Coleman, Jr., E. J. Smith, L. Davis, Jr., D. E. Jones, *Space Research VI*, Proceedings of Sixth Annual COSPAR conference (1965), in press.
3. J. A. Simpson and J. O'Gallagher; J. A. Van Allen and S. M. Krimigis, private communications.
4. E. J. Smith, L. Davis, Jr., P. J. Coleman, Jr., C. P. Sonett, *J. Geophys. Res.* **70**, 1571 (1965).
5. H. S. Bridge, A. Lazarus, C. W. Snyder, private communication.
6. N. F. Ness, *J. Geophys. Res.* **70**, 2989 (1965).
7. H. C. Urey, *Phys. Chem. Earth* **2**, 46 (1957); G. J. F. MacDonald, *J. Geophys. Res.* **67** 2945 (1962); R. A. Lyttleton, *Monthly Notices Roy. Astron. Soc.* **129**, 21 (1965).
8. T. Gold, in *The Solar Wind*, R. J. Mackin and M. Neugebauer, Ed. (Pergamon, New York, 1965).
9. The low field vector helium magnetometer was designed and fabricated by Texas Instruments, Inc., Dallas (F. Reilly, project engineer) under the direction of the Jet Propulsion Laboratory (D. Norris and J. Lawrence, cognizant engineers). Supported by NASA grants and contracts NASw-7 (E.J.S.), NsG426 (L.D.), NGR-05-007-065 (P.J.C.), and NGR-45-001-011 (D.E.J.)

13 August 1965

Occultation Experiment: Results of the First Direct Measurement of Mars's Atmosphere and Ionosphere

Abstract. *Changes in the frequency, phase, and amplitude of the Mariner IV radio signal, caused by passage through the atmosphere and ionosphere of Mars, were observed immediately before and after occultation by the planet. Preliminary analysis of these effects has yielded estimates of the refractivity and density of the atmosphere near the surface, the scale height in the atmosphere, and the electron density profile of the Martian ionosphere. The atmospheric density, temperature, and scale height are lower than previously predicted, as are the maximum density, temperature, scale height, and altitude of the ionosphere.*

Approximately 1 hour after its closest approach to Mars on 15 July 1965, the Mariner IV spacecraft disappeared beyond the limb of the planet, as seen from Earth, and remained in occultation for approximately 54 minutes. Immediately prior to the beginning and immediately after the end of occultation, the spacecraft's S-band radio signal passed through the atmosphere and ionosphere of Mars, both on its way up to the spacecraft, and on its way to Earth after being coherently retransmitted. When this signal reached Earth about 12 minutes later, it marked the first time that a coherent radio transmission has been used to probe the atmosphere and ionosphere of another planet. The changes in frequency, phase, and amplitude of the signal caused by passage through these media have provided new information on the physical properties of the Martian atmosphere and ionosphere.

The acquisition of information to improve the knowledge of the Martian environment has been the objective of the Mariner IV occultation experiment (*1*). Previous knowledge of such atmospheric properties as the surface pressure and density, as well as scale height, is quite poorly defined. The surface pressure, as deduced from recent spectroscopic observations of weak and strong CO_2 absorption bands, was thought to lie somewhere between 10 and 40 mb (*2*). The vertical structure of the atmosphere has not previously been accessible to direct Earth-based measurement and it could only be estimated on the basis of assumption of atmospheric constituents and temperatures. Similarly, the properties of the Martian ionosphere have been the subject of speculation based on the estimated structure of the Martian upper atmosphere, with some models indicating an expected peak electron density of 10^5 to 2×10^7 electrons per cubic centimeter (*3*).

The results of the Mariner IV occultation experiment, when fully analyzed, will provide an improved definition of the surface density and pressure, as well as of the vertical structure of the atmosphere and the electron density profile of the ionosphere, of Mars. However, even a rather superficial analysis, performed in the time since acquisition of the data on 15 July, has yielded significant results.

As the spacecraft approached the limb of the planet, the presence of an atmosphere and ionosphere caused the velocity of propagation of the radio signal to deviate from that in free space because of the nonunity index of refraction of the neutral and ionized media. Also, the radial gradient of the effective index of refraction caused the radio beam to be refracted from a straight-line path. Both of these effects caused the phase-path length of the propagation to differ from what would have been observed in the absence of an atmosphere and ionosphere. Thus, since the geometry obtained from the estimated trajectory is known, the measured deviation in phase can be used to estimate the spatial characteristics of the index of refraction (or refractivity) in the atmosphere and ionosphere by a process of integral inversion or by model fitting (*4*, *5*).

The analysis of Doppler tracking data taken before and after planetary encounter yields the trajectory of the spacecraft at the time of occultation with such precision that the range rate of the spacecraft is known to an accuracy of 0.0015 m/sec. Thus, any significant deviation of the received Doppler data from predictions based on trajectory analysis can be expected to have been caused by atmospheric and ionospheric phase-path effects.

It must be pointed out that the phase changes due to the atmosphere amount to about 30 cycles (wavelengths), and those due to the ionosphere about 10 cycles. They are obtained by subtracting, from the total radio-frequency phase change of about 3×10^{11} cycles during the time period of the experiment, all the predictable phase shift caused by the motion of the spacecraft, reference phase changes, motion of the stations on Earth (3×10^7 cycles), light-transit time effects, the effects of Earth's troposphere, and others. Thus, it is implied that the total phase change due to all causes other than the atmosphere and ionsophere of Mars must be known to an accuracy of less than 1 part in 10^{11}.

Before discussing the data obtained in this manner, we will describe the geometry of occultation for both entry and exit. At entry into occultation, the spacecraft was at a distance of 25,570 km from the limb of Mars, traveling at a velocity of 2.07 km/sec normal to the Earth-Mars line. The point of tangency on the surface of Mars was at a latitude of 55°S and a longitude of 177°E, corresponding to a point between Electris and Mare Chronium. At the time of exit from occultation, the distance from the limb of Mars had increased to 39,130 km, and the point of tangency was located at about 60°N and 34°W, falling within Mare Acidalium.

Doppler and amplitude data were taken both during entry and exit by the NASA/JPL Deep Space Instrumentation Facilities (DSIF) at Goldstone, California, and Tidbinbilla and Woomera, Australia. The Goldstone stations (Echo and Pioneer) took standard tracking Doppler (closed-loop) as well as open-loop records (described below) of the received signal. The Australian stations took only Doppler data. At entry all data were taken while the spacecraft's transmitter frequency reference was provided by a frequency standard on Earth. At exit, a portion of the data was received while the spacecraft's transmitter frequency reference was provided by an on-board crystal oscillator. In the latter mode, the precision of phase measurements is significantly degraded.

Figure 1 shows the observed minus the predicted phase change in 1 second based on data received at the various DSIF stations. The points marked O/L have been obtained from the open-loop records by means of spectral density analysis, and the other points are derived directly from data processed through the JPL orbit-determination

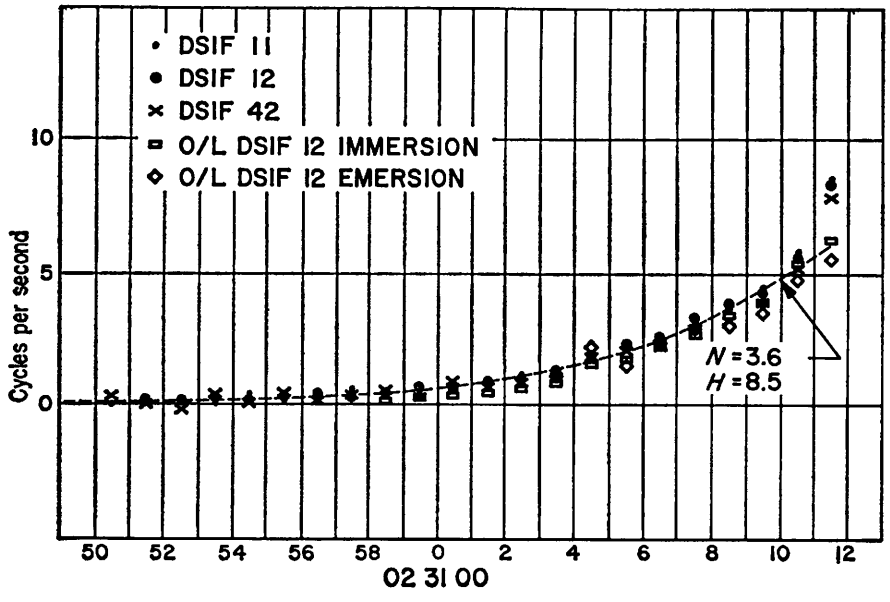

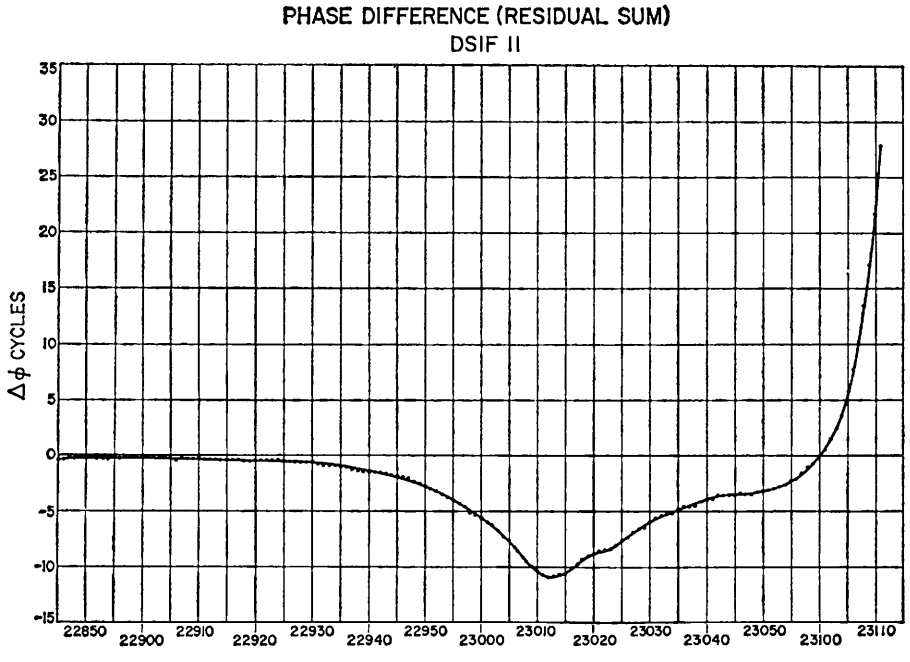

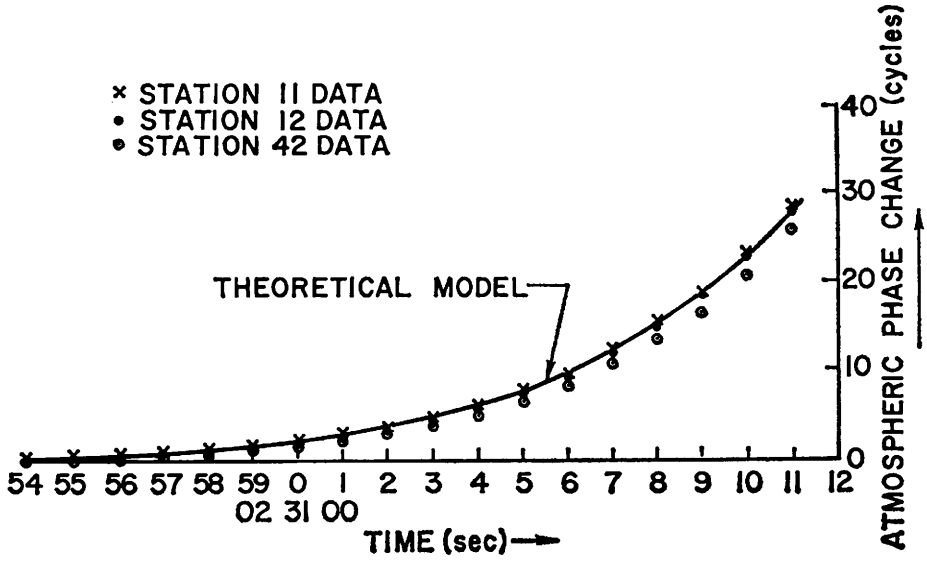

Fig. 1 (top). Doppler residuals. The observed minus the predicted phase changes in 1 second. Abscissa is U.T. 15 July.
Fig. 2 (center). Relation of total phase change to time. Abscissa is U.T. 15 July.
Fig. 3 (bottom). Portion of graph of Fig. 2 in neutral atmosphere.

program. One may observe that the data from the various sources show a high degree of consistency, except for the Doppler points at 02:31:11.5, which are suspect because the time of loss of signal is estimated to be between 02:31:11.2 and 02:31:11.6 U.T.

A different presentation is shown in Fig. 2, which represents the total phase change as a function of time, derived from station 11 (Goldstone-Pioneer) Doppler residuals. The maximum effect of the ionosphere appears at about 02:30:10, and the final upswing, beginning at about 02:30:50, is caused by the neutral atmosphere. It is interesting to note the extreme smoothness of data suggested by the low scatter of the points.

An expanded portion of the phase-change plot is shown in Fig. 3. This graph relates only to the neutral atmosphere, as the effects of the ionosphere have been removed. Signal extinction time is assumed as 02:31:11.2.

The solid curve represents the computed phase change for a theoretical exponential model atmosphere having a surface refractivity (N) of 3.7 N units and a scale height of 9 km. Even with this relatively crude model the fit is excellent. The dotted line in Fig. 1 represents the computed Doppler residuals for a similar model atmosphere, having a scale height of 8.5 km and $N = 3.6$. As in the case of the phase change, the fit of the data appears to be quite good.

Figure 4 relates maximum phase change, maximum frequency change (Doppler), and refractive gain (at the time of extinction of the signal of 02:31:11.2) to the surface refractivity and scale height of an exponential density model of an atmosphere. Suggested values of 5.5 ± 0.5 cy/sec, 29 ± 2 cy, and 1.5 to 2.0 db lead to the stippled area in the figure. This area corresponds to a surface refractivity of 3.6 ± 0.2 N units and a scale height of 9 ± 1 km. The gain figure is least reliable, but it can be seen that better values from detailed analysis of data from all the stations should help considerably in reducing uncertainty. In addition, the

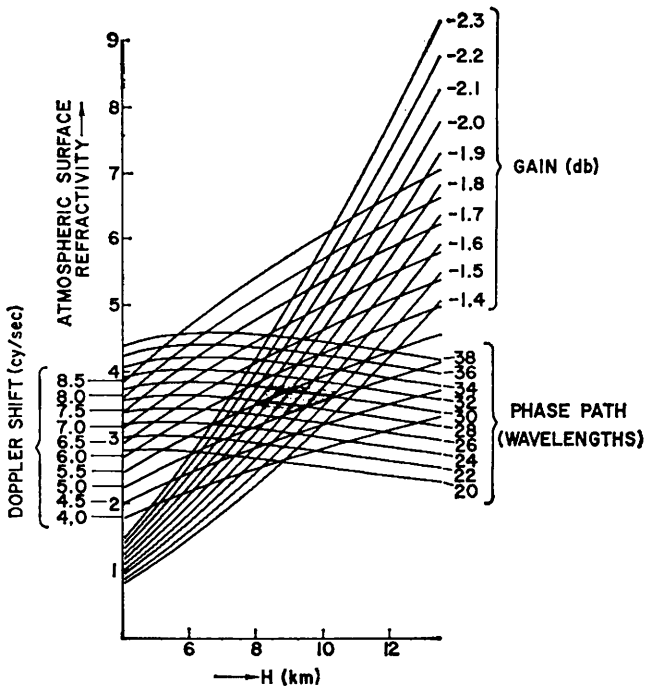

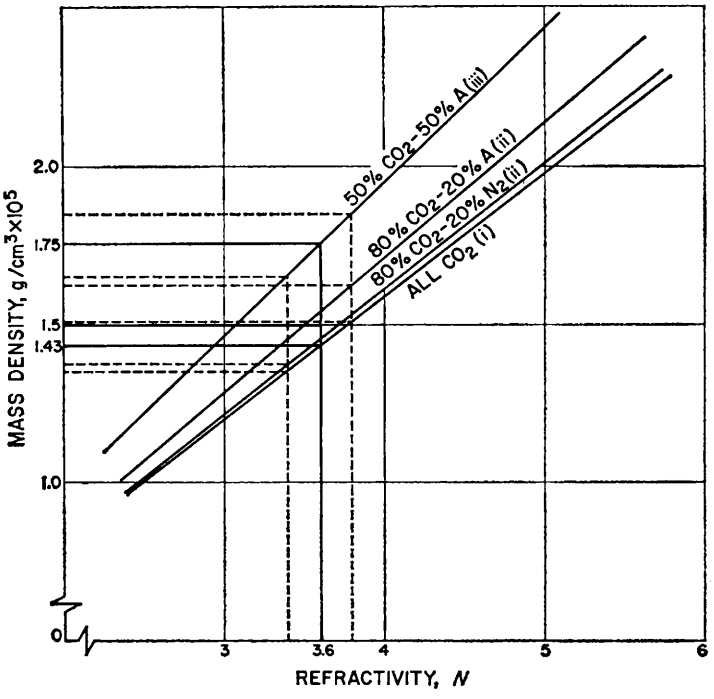

Fig. 4 (left). Maximum changes of phase and frequency in relation to refractivity and scale height of model atmospheres. Fig. 5 (right). Refractivity and mass density as a function of atmosphere composition.

measurements of the Fresnel diffraction pattern should provide an independent set of contours parallel to the gain curves for further refinement (*5*).

A cursory study of the Fresnel pattern in the amplitude recordings leads us to believe that signal dropout was due to a diffracting edge, establishing the very important fact that the final ray paths grazed a surface feature on Mars. All references to surface conditions in this report refer to the altitude of this surface feature. We do not know, of course, its altitude relative to the mean surface of Mars, but the geometry of the experiment would make it likely that it was higher than the mean surface. The mean surface density and pressure would be about 1 percent larger than the values given here for each 90 m of height of the occulting feature above the mean surface level.

So far, analysis shows no obvious change of scale height with altitude to about 30 km.

In essence then, a simple refractivity model of the Martian atmosphere has been established. It now remains to infer density and pressure, thus bringing into focus the question of composition and temperature.

Figure 5 shows the relation between refractivity and mass density as a function of composition, ranging from pure CO_2 to 50 percent CO_2 and 50 percent argon. Since the Martian atmosphere contains spectroscopically measurable amounts of CO_2, and the scale height has been established to about 8 to 10 km, it can be reasonably assumed that the atmosphere consists primarily of CO_2.

Three models differing in composition are considered here: (i) pure CO_2; (ii) 80 to 100 percent CO_2 and the rest argon or nitrogen, in any proportion; and (iii) 50 percent CO_2 and 50 percent argon.

For the atmosphere composed of pure CO_2 (model i) the total number density at the surface, corresponding to the measured refractivity values stated above, was about $1.9 \pm 0.1 \times 10^{17}$ molecules per cubic centimeter (mol/cm^3). The mass density (Fig. 5) is then about $1.43 \pm 0.10 \times 10^{-5}$ g/cm^3. From the measured value of scale height, the temperature range would have to be about $180° \pm 20°$K, leading to a surface pressure range of 4.1 to 5.7 mb.

For atmosphere model ii (80 to 100 percent CO_2), the number and mass densities are $2.1 \pm 0.2 \times 10^{17}$ mol/cm^3 and $1.5 \pm 0.15 \times 10^{-5}$ g/cm^3, respectively. From the assumed percentage

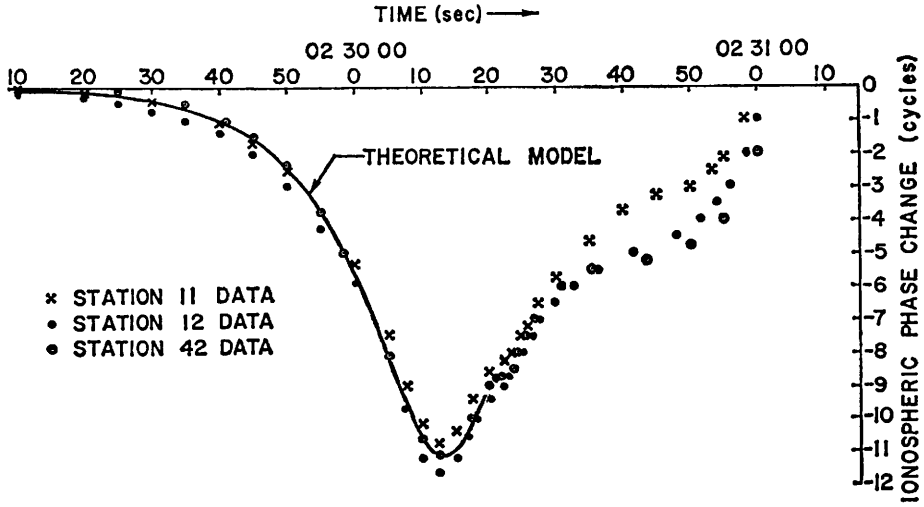

Fig. 6. Phase-path change as spacecraft moved behind ionosphere.

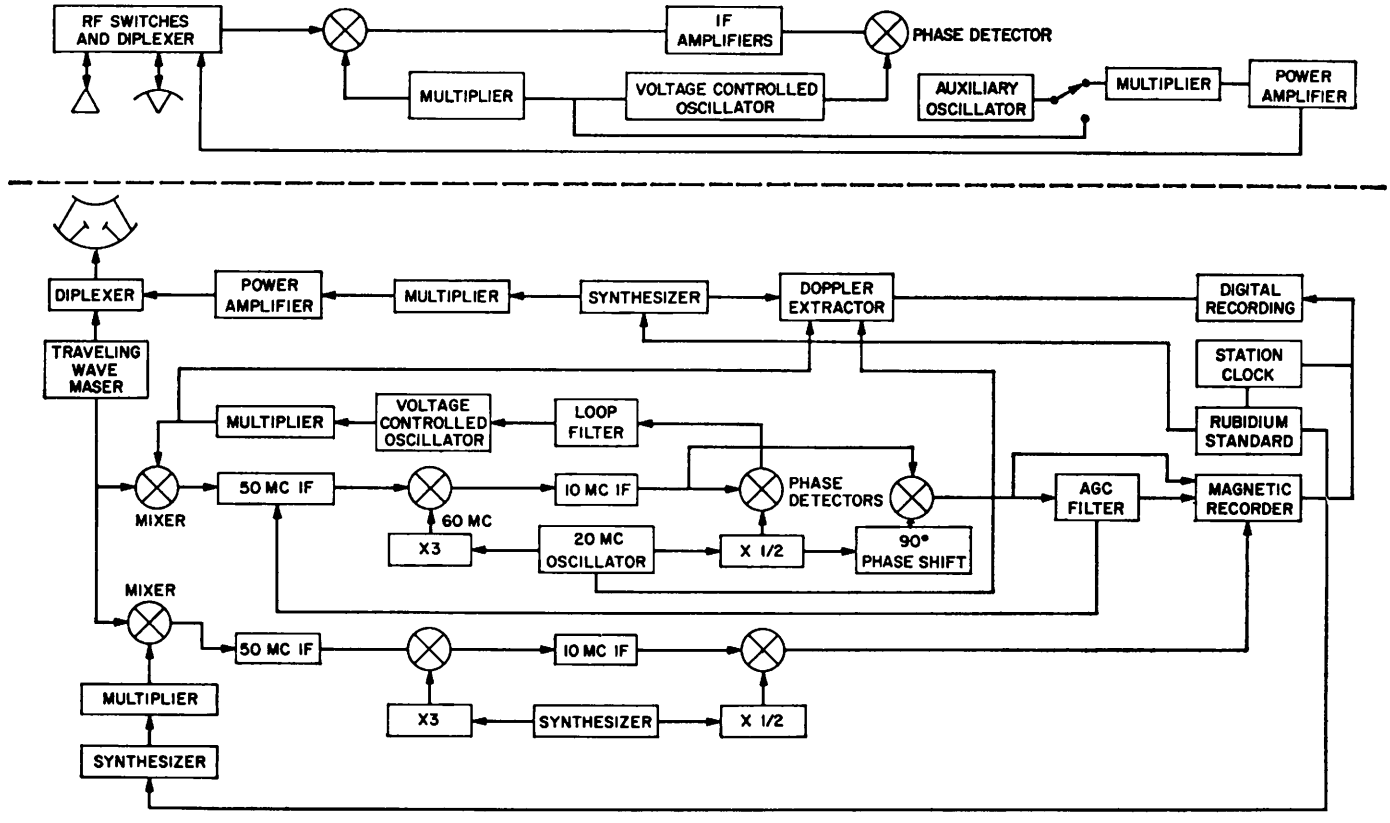

Fig. 7. Block diagram of DSIF radio system. MC, megacycles; X, times; IF, intermediate frequency; AGC, automatic gain control.

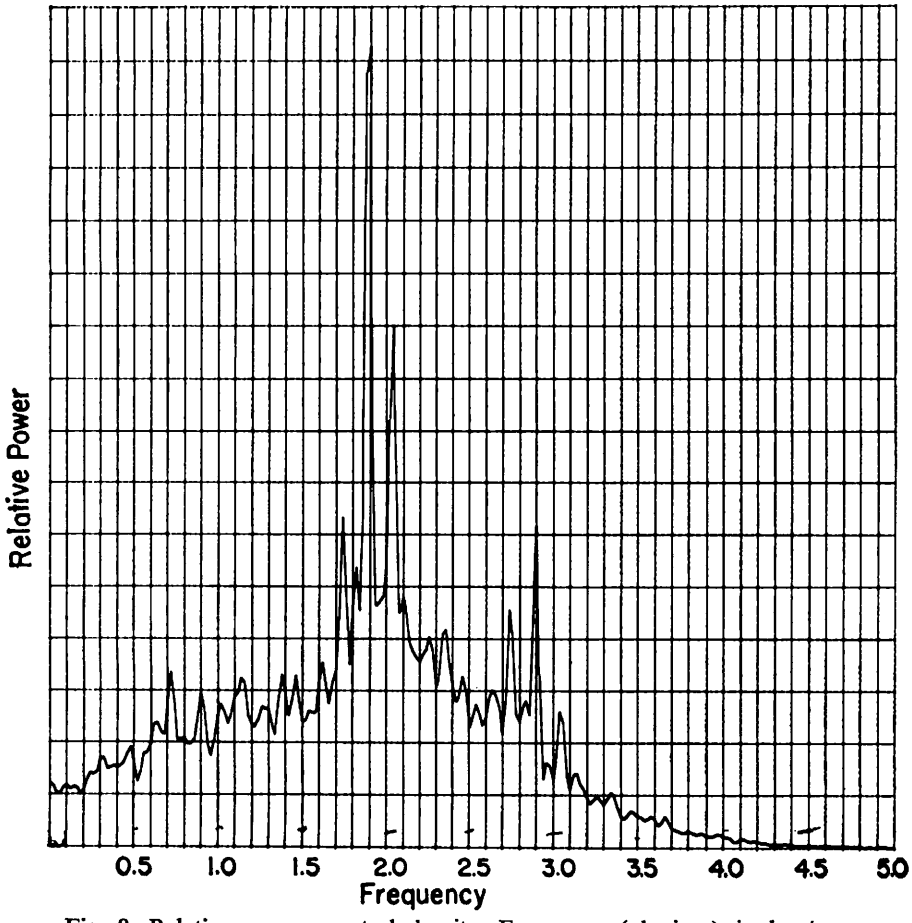

Fig. 8. Relative power spectral density. Frequency (abscissa) in kcy/sec.

of the other constituents, as well as the scale height, the temperature range is 175° ± 25°K, leading to a surface pressure of between 4.1 and 6.2 mb.

Finally, for the atmosphere having equal partial pressures of CO_2 and argon (model iii), the various properties are as follows: number density = $2.5 \pm 0.15 \times 10^{17}$ mol/cm^3; mass density = $1.75 \pm 0.1 \times 10^{-5}$ g/cm^3; temperature = 170° ± 20°K; and surface pressure = 5.0 to 7.0 mb.

The number densities derived for these models correspond to from 0.7 to 1.0 percent of the molecular number density of Earth's atmosphere at the surface. Since the scale height in the Martian atmosphere is apparently almost equal to that of Earth, the total number of molecules above a unit area on the surface of Mars is also on the order of 1 percent of that on Earth.

Figure 6 shows the change in two-way phase path as Mariner moved in behind the Martian ionosphere above Electris. Data from stations 11, 12, and 42 are all plotted in the same figure.

The local time was afternoon, and the sun was about 20 degrees above the horizon at the time when the S-band signal probed through this portion of the Martian atmosphere.

From the ionospheric phase-path data, one can determine the distribution in height of the electron density, $F(h)$. The electron-density profile may be calculated either from inversion of the integral equation relating the phase path to $F(h)$ or by curve-fitting or by both (*4–6*). A combination of these techniques is being used to determine the electron-density profile from the phase-path data.

Analysis of the data at this time indicates a distinct ionospheric layer with an electron-density peak of about 9×10^4 electrons per cubic centimeter (el/cm^3) at an altitude of about 125 km. The electron scale height above this peak is 20 to 25 km. (The neutral scale height is half this value.) The curve labeled "theoretical model" in Fig. 6 shows the phase path one would measure with this electron-density profile.

Both the small scale height above the electron-density peak and the low altitude of the peak, together with the small scale height in the neutral region near the surface, suggest that the Martian atmosphere is considerably cooler than previously anticipated.

The preliminary conclusion regarding the preponderance of CO_2 in the lower atmosphere also appears to be reasonably consistent with the ionospheric measurements, since high abundances of CO and O (resulting from the dissociation by solar radiation) indicate more effective radiative cooling than previous estimates (based on N_2 as the main constituent) suggested for the upper atmosphere of Mars.

The phase path data shown in Fig. 6 were taken when the spacecraft entered occultation. A preliminary analysis of the data obtained during exit does not show a detectable ionosphere. Thus, the nighttime (solar zenith angle 106°) electron density over Mare Acidalium is lower than the daytime density by at least a factor of 20.

There is a suggestion of a minor peak at the height of about 95 km. The two layers may correspond to E and F regions in the Martian ionosphere. It is interesting to note, although no doubt a happenstance due to the mixture of widely varying conditions, that the main Martian layer is very similar in electron density, scale height, and altitude to the normal E region of Earth's ionosphere. The data from below the peak also show evidence of nonspherical symmetry, as would be expected from the variable illumination along the ray path. We believe the maximum number density given above is correct to about 10 percent.

The ionospheric profile does not differ markedly from that expected if there were a Chapman layer above the peak. If the profile follows the well-known variations for this simplified model, the peak density at a solar zenith angle 0° would be 1.5×10^5 el/cm^3, corresponding to a critical frequency of 3.5 Mcy/sec, as compared with 2.7 Mcy/sec at 70° zenith angle. The total ionospheric contents along a vertical column would be 5×10^{11} el/cm^2 at 70° and 7×10^{11} el/cm^2 at 0°. Corresponding daytime densities in Earth's ionosphere are on the order of 10^6 el/cm^3, and vertical contents are about 10^{13} el/cm^2 with very large diurnal, seasonal, latitudinal, and sunspot-cycle variations. Temperatures in Earth's main ionospheric layer are approximately an order of magnitude larger than in this Martian layer.

There still remains some possibility that more detailed studies of the phase path will show some ionization at greater heights. There is a slight suggestion of this in the preliminary data. However, the number density would be very low in such a layer, if it exists.

The near or complete absence of a static magnetic field on Mars has very interesting implications with regard to understanding the ionosphere and atmosphere of both Mars and Earth. For Mars, it means that one can better understand formation and loss mechanisms and better relate these to the physical characteristics of the atmosphere and ionosphere, since there are no complicating effects of such a field. For Earth, many ionospheric phenomena are still not well understood, often because of the complicating effects of the magnetic field in controlling incoming charged particles, in affecting ionospheric motions, in storing high-energy particles which may provide a heating and ionization source, in affecting and controlling small- and large-scale ionospheric irregularities, and in providing partial shielding from the solar wind. Results of studies of the Martian ionosphere should thus help in separating and understanding various phenomena in Earth's ionosphere.

The results described have been derived from frequency, phase, and amplitude measurements at the DSIF receiving stations during the occultation experiment. To better understand these measurements, it will be helpful to have a brief description of the DSIF radio system, including the special modifications for the experiment. The block diagram of the system is illustrated in Fig. 7.

The ground station uses a rubidium standard to drive a frequency synthesizer. Its output is then modulated, multiplied 96 times in frequency, amplified, and transmitted to the spacecraft at 2.1 Gcy/sec. When the spacecraft receiver is in lock with the ground-station signal, the down-link frequency is derived from the receiver's voltage-controlled oscillator (VCO), which is phase-locked to the

Table 1. Summary of occultation experiment.

Atmosphere	
Surface refractivity	3.6 ± 0.2 N units
Scale height	8 to 10 km
Surface number density	
100% CO_2	$1.9 \pm 0.1 \times 10^{17}$ mol/cm^3
Up to 20% A or N_2, or a mixture	$2.1 \pm 0.2 \times 10^{17}$ mol/cm^3
50% A	$2.5 \pm 0.15 \times 10^{17}$ mol/cm^3
Surface mass density	
100% CO_2	$1.43 \pm 0.1 \times 10^{-5}$ g/cm^3
Up to 20% A or N_2, or a mixture	$1.5 \pm 0.15 \times 10^{-5}$ g/cm^3
50% A	$1.75 \pm 0.10 \times 10^{-5}$ g/cm^3
Temperature	
100% CO_2	180 ± 20°K
Up to 20% A or N_2, or a mixture	175 ± 25°K
50% A	170 ± 20°K
Surface pressure	
100% CO_2	4.1 to 5.7 mb
Up to 20% A or N_2, or a mixture	4.1 to 6.2 mb
50% A	5.0 to 7.0 mb
Ionosphere	
Maximum electron density ($\chi = 70°$)	$9 \pm 1.0 \times 10^4$ el/cm^3
Altitude of maximum	120 to 125 km
Electron scale height above maximum	20 to 25 km
Temperature	<200°K at 120 to 200 km

received up-link signal. When no up-link is received, however, the down-link frequency is derived from a free-running crystal oscillator in the spacecraft. The radio frequency signal is amplified and transmitted from a high-gain spacecraft antenna.

The ground transmitter and receiver system employs an 85-foot (26-m) parabolic antenna with a Cassegrainian simultaneous-lobing feed. A traveling-wave maser cooled by a closed-cycle helium refrigerator operating at 4.2°K is used for the receiver front end. After amplification by the maser, the signal is split into two separate receiver channels. The first channel consists of a triple-conversion phase-locked receiver. It is operated in the standard DSIF receiver configuration. This receiver's VCO is kept in phase synchronism with the received signal. By a series of frequency multiplications, divisions, and additions, the transmitter's exciter frequency is coherently compared to the receiver's VCO to obtain the two-way Doppler frequency. The receiver's automatic gain control (AGC), which is a received-signal power-level tracking servo, is used to determine received-power level. Appropriate AGC voltages were recorded on magnetic tape, and the Doppler count was digitized. This system yielded frequency information in real time. This channel is also used as the sum channel of the pointing system for the simultaneous-lobing antenna.

The second receiver channel—a manually tuned, constant-gain, triple-conversion superheterodyne—is operated in a nonstandard configuration. It amplifies and translates the down-link signal to the audiofrequency region of the spectrum and then records it on magnetic tape. The local-oscillator (LO) signals for this receiver were derived from the rubidium frequency standard, which drives a pair of synthesizers. The first LO frequency was periodically stepped to keep the signal in the receiver's passband. The second and third LO's were derived from the second synthesizer operating at 19.996 Mcy/sec. The output of the third mixer had a passband of 1 to 3 kcy/sec, which was recorded on magnetic tape. Since the LO frequencies are derived from the rubidium standard, the frequency integrity of the Doppler is maintained. The analog information on the magnetic tape was digitized after the mission for use in a digital computer.

Figure 8 is a power spectrum of the audio open-loop signal made from the digitized tape on an IBM 7094 computer. The time interval from 03:25:16 to 03:25:17 was chosen. During this second, the one-way frequency, which was first observed as the vehicle reappeared at 03:25:08, was switched off. (This signal component can be seen at 2900 cy/sec.) After the one-way signal disappeared, the two-way signal was recorded at an audio frequency of 1900 cy/sec. The phase modulation sidebands at ± 150 cy/sec can be seen on both signals.

It should again be pointed out that these numbers are the results of less than 1 month's analysis with relatively crude techniques. As the analysis proceeds, the results will be refined, taking into account additional data as well as more sophisticated theoretical investigations of the physical characteristics of the atmosphere and ionosphere.

ARVYDAS KLIORE
DAN L. CAIN, GERALD S. LEVY
Jet Propulsion Laboratory, California Institute of Technology, Pasadena

VON R. ESHLEMAN
GUNNAR FJELDBO
Center for Radar Astronomy, Stanford University, Stanford, California

FRANK D. DRAKE
Department of Astronomy, Cornell University, Ithaca, New York

References and Notes

1. A. J. Kliore, D. L. Cain, G. S. Levy, V. R. Eshleman, F. D. Drake, G. Fjeldbo, *Astronaut. Aeronaut.* **7**, 72 (1965). The occultation experiment has been conducted by investigators at JPL, Stanford University, and Cornell University.
2. L. D. Kaplan, G. Munch, H. Spinrad, *Astrophys. J.* **139** (1964); G. P. Kuiper, Mars issue, *Comm. Lunar Planetary Lab.* **2**, 79 (1964), Univ. of Arizona.
3. R. B. Norton, *NASA TN-D-2333* (NASA Code AFSS-A, Washington, D.C., 1964).
4. A. Kliore, D. L. Cain, T. W. Hamilton, *J.P.L. Tech. Rept. No. 32-674* (Jet Propulsion Laboratory, Pasadena, Calif., 1964); G. Fjeldbo, *Final Report NSF G-21543, SU-SEL-64-025* (Stanford University, Stanford, Calif., 1964).
5. G. Fjeldbo and V. R. Eshleman, *J. Geophys. Res.*, **70**, 13 (1965).
6. G. Fjeldbo, V. R. Eshleman, O. K. Garriott, F. L. Smith, III, *ibid.*, p. 15.
7. We thank the Mariner Project and Deep Space Net personnel of JPL for their excellent performance in the preparation for the experiment and the acquisition of data. Also, special gratitude is due T. W. Hamilton of JPL and B. B. Lusignan of Stanford University for their many contributions to the success of the experiment. This paper presents the results of one phase of research carried out at the JPL, California Institute of Technology, under NASA contract NAS 7-100. The Stanford contribution was supported under NASA contracts NGR 05-020-065 and NsG-377.

23 August 1965

Heat Stabilities of Acid Phosphatases from Pinto Bean Leaves

Abstract. *Two acid phosphatases were demonstrable by polyacrylamide gel electrophoresis. They had different mobilities and different heat stabilities in 1.0*M *acetate buffer,* p*H 5.2. Both phosphatases had the same electrophoretic mobility in tris buffer at* p*H 7.5, gave one boundary in the analytical ultracentrifuge in tris or acetate buffer, and had the same sedimentation coefficient. The difference in these properties suggests an alteration in conformation of the proteins by the buffer systems.*

Newer techniques of protein chemistry, especially starch gel and polyacrylamide gel electrophoresis, have spurred the study of protein changes that occurr in plant and animal organs during disease or ontogeny. We have been studying acid phosphatase changes in bean leaves after removing the terminal buds. The heat stability of this enzyme was found useful in its characterization. These studies raised the possibility that there were two acid phosphatases which differed in their stability to heat. Heat stability studies also suggest the occurrence of multiple acid phosphatases in other tissues (*1*).

Acid phosphatase was extracted from bean leaves (*Phaseolus vulgaris* L. var. Pinto) and highly purified (*2*). A 1.0*M* acetate buffer, *p*H 5.2, was employed as the extraction medium and a freeze-thaw cycle, carried out at *p*H 5.2, was introduced before column chromatography on diethylaminoethyl cellulose at *p*H 7.5 in 0.01*M* tris (hydroxymethyl) aminomethane-HCl (tris) buffer. Enzyme activity was assayed by the method of Torriani (*3*) and protein was determined by the micro-Kjeldahl technique (*4*). The enzyme had a broad substrate range, *p*H optimum at 5.2, and hydrolysis of *p*-nitrophenylphosphate was noncompetitively inhibited by fluoride (*2*). Thus the enzyme is a typical type II phosphomonoesterase.

Loss in enzyme activity on heating in 1.0*M* acetate buffer, *p*H 5.2, is shown in Fig. 1. The initial decay in acetate buffer is approximately first order, but the drop in activity stops after 40 minutes, which suggests that two enzymes were present in the enzyme preparation, one of which was less heat